AN *AB INITIO* INVESTIGATION OF THERMOELASTIC PHASE

TRANSFORMATIONS IN TRANSITION METAL ALLOYS

A Dissertation

by

ANJANA ANA TALAPATRA

Submitted to the Office of Graduate and Professional Studies of
Texas A&M University
in partial fulfillment of the requirements for the degree of

DOCTOR OF PHILOSOPHY

Chair of Committee,	Raymundo Arróyave
Committee Members,	Ibrahim Karaman
	Tahir Çağin
	Xinghang Zhang
Head of Department,	Andreas A. Polycarpou

December 2015

Major Subject: Mechanical Engineering

ABSTRACT

The energy pathways associated with the martensitic transformation in shape memory alloys (SMAs), though the focus of extensive research over the past decades, are still unclear. In this work, we use a first-principles approach within the framework of density functional theory, as implemented in the Vienna *ab initio* simulation package (VASP), to model the transformation in transition metal alloys by tracking atomic motion via shear, shuffle and distortion during the transformation. We build a framework to investigate the f.c.c-h.c.p transformation in Co-based binary alloys which may be applied to ternary alloys as well. In the Co_2NiGa Heusler system, by applying the Burgers transformation, we found a low-energy phase with orthorhombic symmetry (O) phase which is lower in energy than the experimentally observed $L1_0$. By performing a detailed analysis of the transformation paths (Burgers and Bain) taking into account perturbations on the ground state, it is seen that a phase selection problem exists: the ultimate crystal structure that the system transforms into, depends on the path that the system prefers. When coming from high temperature, the accessible path is that corresponding to the Bain transformation. Finally, we present a complete and unique 4-parameter model to describe the $B2 - B19'$ transformation in $Ni - Ti$. We eliminate the possibility of the $B19$ phase being an intermediate phase in the transformation and show that it is in fact a barrierless transformation. Crystallographic analysis of intermediate states shows that the $B2 - B19'$ path follows a known crystallographic path.

DEDICATION

To the giants,

It has been a privilege to stand upon your shoulders

ACKNOWLEDGEMENTS

Pritha has been the constant in my life and I would like to thank her for being herself and always being there for me. Most importantly, thank you for introducing me to my future husband. I am indebted forever. Purvee, thank you for holding on even when I was far away. Abhilasha - thank you for teaching me how to schedule fun and naps between concentrated bursts of work and for being the best kind of friend. Nikhil and Sneha, thinking of you both always makes me smile. Anand Govindsamy is the most incredible and original person I have encountered in my life, and I cherish his friendship. Thank you for the music, the late nights and the garbage drive-bys. Saradhi, Guru and Ajit, thank you for your friendship.

Shriram Srinivasan, my husband, has been my friend, my teacher, my voice of reason, an inspiration and always, a person worth revering. Thank you for letting me be myself, for loving me for the right reasons, for your consistency and your continued support. I look forward to a lifetime of love, laughter, travel and hard work with you. To my mother-in-law, thank you for your prayers and for wanting the best for me always. To my parents, thank you for making me the person I am today, for the all-encompassing love, the faith and for instilling in me a desire to always stay true to myself. Baba, thank you for always having the answer, for being Superman and for never failing me. Ma, thank you for the happiest childhood any child could ever ask for, for all the music and the stories. To Aruna, my sister, thank you for the unconditional love. Thank you for finding my notebooks and textbooks every single time. Thank you for being the sister I have always looked up to. Nayeem, thank you for being the brother I never had. Thank you for loving me, being proud of me and for making me invest my money. Nadia, I look at the marvel that you are and am just amazed. You are the brightest star in my universe and in many ways, show me the way ahead. Amma and Mesho, I miss you both every single day. Thank you for everything, all my memories begin with you.

NOMENCLATURE

MT   Martensitic Transformation

SMA   Shape Memory Alloy

SME   Shape Memory Effect

M_s Martenistic start temperature

DFT   Density functional theory

H-K   Hohenberg-Kohn

MEP   Minimum Energy Path

SN   Shoji-Nishiyama

WL   Wenkovitch-Lam

MHM   Minima Hopping Method

EPN   Ericksen-Pitteri Neighbourhood

TABLE OF CONTENTS

LIST OF FIGURES

LIST OF TABLES

1. INTRODUCTION

The martensitic transformation (MT) is a diffusionless solid-solid phase transformation which occurs by a cooperative movement of atoms. Diffusionless phase transformations are structural transformations characterized by a small change in atomic positions, typically within one interatomic distance. The change in structure is abrupt and is characterized by a specific temperature, composition, and pressure. The microscopist Adolf Martens in 1890 observed martensite for the first time under the microscope and the phase was named after its discoverer [1]. Martensite is observed on rapid cooling of a high temperature phase by thwarting the development of the low-temperature phase. Consequently it is a non-equilibrium phase. The high-temperature symmetric phase is known as austenite (so named after the metallurgist William C. Roberts-Austen) and transforms to a low-symmetry, low-temperature phase when cooled. Since martensite is generated by atom movement, it results in the induction of many lattice imperfections such as dislocations, stacking faults and twin faults. Martensitic phase transformations are found to occur in almost all pure metals and metallic alloys of the group III-IV of the periodic table of the elements as well as few other materials and ceramics [2]. A complete and cogent discussion of martensitic transformations is beyond the scope of this work. The interested reader may refer to the excellent foundational book by Z.Nishiyama [3] for a thorough discussion.

Through the march of the centuries, the quest for better materials to simplify the life of man has continued uninterrupted. Fueled by technological advances, growing populations, and the consequent pressure on the ecology, the field of materials science prospers. Advances in materials still have the ability to surprise and delight us, much
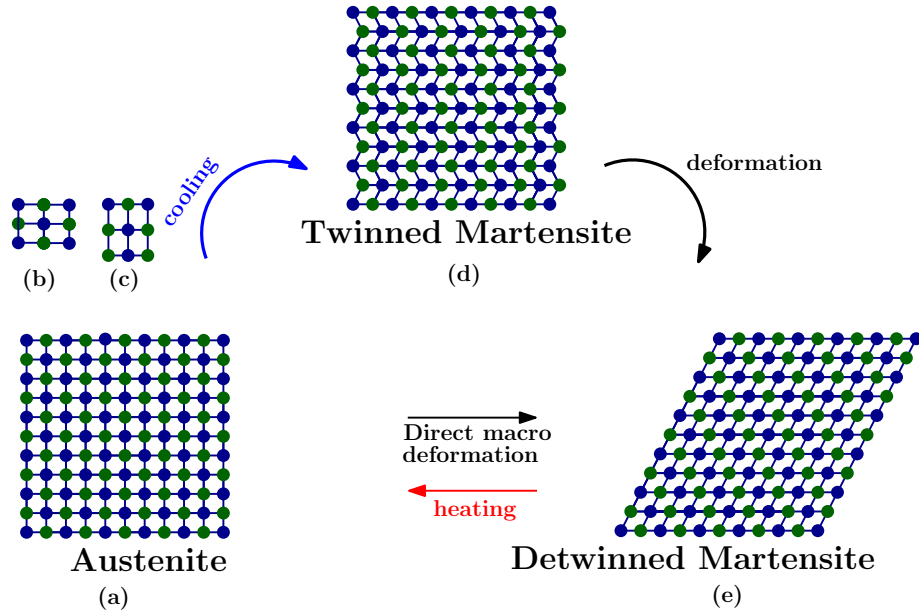
Figure 1.1: Schematic illustration of the shape memory effect

in the same way they delighted early man thousands of years ago.

One such unique class of materials are shape memory alloys which can recover apparent plastic strains when subjected to some form of external stimuli such as heat, stress or magnetization. A solid-solid phase transformation (the martensitic transformation), occurs wherein the material undergoes a change in crystal structure. The 1950's saw the discovery of the shape memory effect (SME) as observed in the Au-Cd [4] and the In-Tl [5] systems. The discovery of the Ni-Ti SMA in 1963 [6] provided impetus to the interest in research on shape memory alloys. By 1970, it was established that the shape memory alloys (SMAs) are a sub-group of alloys which undergo a thermoelastic martensitic transformation [7]. Since then, a large number of investigations have been carried on the SME and it's accompanying effects.

In Figure 1.1 the shape memory effect is illustrated schematically. In (a) the SMA is in the high temperature austenitic phase. When cooled, the austenite struc-

turally transforms into the low temperature structure in (b). This low temperature martensite may have variants as shown in (b) & (c). To minimize it's energy, the SMA transforms into a mixture of variants, giving rise to the twinned martensitic structure seen in (d). This twinned martensite can be easily deformed as in (e). At this stage, if the alloy is heated again, the deformed martensite transforms back into high-temperature, high-symmetry austenite.

Shape memory alloys thus exhibit a reversible martensitic transformation. The reversibility of the transformation depends on the order of the transformation. Second-order transformations such as order-disorder, magnetic or dielectric transformations are reversible. First-order transformations may be reversible if the lattice constants of the parent and product structures are such that the martensite may grow in the austenite phase without creating long-range stress. While undergoing a martensitic transformation, the austenite can give rise to several martensite variants which may combine in twinning and deformation. However, each of these variants or combinations thereof return to a unique parent austenite. The material during the course of the transformation is always within a neighbourhood such that it is able to store the data necessary to 'remember' the way back to the parent martensite. It is essential that the material remain within this neighbourhood, called the 'Ericksen-Pitteri' neighbourhood (EPN) in order to exhibit the shape memory effect.

Nearly all phase transformations in solid metals and alloys are heterogenous processes and can be classified as i)reconstructive or ii) displacive transformations [8]. Reconstructive tranformations encompass a change in the primary coordination and are second order phase transitions. The transformed phase is not a subgroup of the parent phase and there is no associated energy barrier. Displacive transformations occur by the ordered and correlated motions of atoms accompanied by a change in the secondary coordination. The transformed phase is a subgroup of the parent phase.

3

The martensitic transformation in SMAs may be modeled as displacive transformations. The transition is of first order and is a barrier overcoming process. Displacive martensitic transformations thus have an associated energy barrier which characterizes them. The energy barrier indicates the energy required for the transformation to occur and thereby defines the martensitic transformation temperature.

For the purposes of this work, it is also essential to make a distinction between thermoelastic and athermal martensitic transformations. The thermoelastic martensitic transformation is one in which the martensite grows continuously on lowering of temperature and diminishes continuously on raising of the temperature [9]. In a thermoelastic transformation, the chemical driving force and the resistive stored elastic energy must proceed more or less in equilibrium. The transformation may see abrupt transitions whenever the chemical driving forces exceed the resistive forces. The athermal transformation (as in most steels) proceeds only with change in temperature and the reaction stops when the temperature is kept constant. The TTT (time-temperature-transformation) phase diagrams may be used to account for the amount of isothermal martensite for a particular holding time and temperature [10, 11].

In spite of being such a universal phenomenon, and even though there has been an interest in the transformation for over a 100 years, it is not very well understood even today. While a few simple models exist to explain the transformation in pure metals and alloys, there are a great number of metals and alloys in which the transformation pathways are unexplained. As described by Cohen[1]; '*Martensitic transformations are diffusionless structural transitions which are shear-dominant and lattice distortive. The morphology and the kinetics are mainly determined by the strain energy*'. Consequently, the models that do exist are a combination of shears, shuffles and distortions.

In this dissertation we present a cogent and comprehensive analysis of the marten-

sitic transformation mechanism from a structural viewpoint to gain an insight into the driving forces behind the transformations in three different SMA systems: (i) Co-based binary SMAs, (ii) Co-Ni-Ga high temperature shape memory alloy (HTSMA), and (iii) Ni-Ti binary SMA. In Section 3 we debate the applicability of the Bain transition mechanism in the case of Co-based alloys and show the energetics of the Bain path in the Co - Al system. Two phenomenological models for the f.c.c to h.c.p transformation are discussed and applied to the binary Co - Al, Co-Si and Co-Fe binary alloys. The minimum energy paths (MEPs) for the transformations are calculated and are compared with experimental data. In Section 4, an extensive *ab initio* study of the transformation paths in the martensitic Co_2NiGa system is carried out. Possible transformation mechanisms are studied and it is shown that the initial L_{21} structure may transform either to the $L1_0$ or the 0 structures. Although the O structure corresponds to lower total energy, several phenomena can lower the total energy of $L1_0$ and make it comparable to that of the O structure. The latter has not been observed experimentally and an extensive analysis is carried out to determine the energetics which render the $L1_0$ phase lower in energy. In Section 5, we present a first-ever consolidated four-paramter model for the $B_2 - B19$ martensitic transformation in Ni-Ti. We show that the $B19$ phase, while crystallographically possible, is not a likely intermediate phase in the transformation. Finally, the MEP for the four-parameter model is calculated and it is shown the obtained path is a viable crystallogrpahic route. Computational methods used in this work are described in the following section.

2. METHODOLOGY AND COMPUTATIONAL TECHNIQUES

2.1 Density Functional Theory (DFT)

The year 1926 saw the publishing of Erwin Schrödinger's epoch-making paper[12] introducing wave mechanics. It introduced the Schrödinger equation, a partial differential equation (PDE) describing the evolution of the wave function of a physical system. The goal of most appproaches in solid state physics and quantum chemistry is to solve the time-independent, non-relativistic Schrödinger equation:

$$\hat{H}\psi_i(\vec{x_1}, \vec{x_2}, ...\vec{x}_N, \vec{R}_1, \vec{R}_2....\vec{R}_M) = E_i\psi_i(\vec{x}_1, \vec{x}_2, ...\vec{x}_N, \vec{R}_1, \vec{R}_2....\vec{R}_M) \qquad (2.1)$$

where $\hat{H}$ is the Hamiltonian for a system consisting of M nuclei and N electrons, ψ is the wavefuction and E is the constant energy. The Hamiltonian $\hat{H}$ is given by:

$$\hat{H} = -\frac{1}{2}\sum_{i=1}^{N}\nabla_i^2 - \frac{1}{2}\sum_{A=1}^{M}\frac{1}{M_A}\nabla_A^2 - \sum_{i=1}^{N}\sum_{A=1}^{M}\frac{Z_A}{r_{iA}} + \sum_{i=1}^{N}\sum_{j>i}^{N}\frac{1}{r_{ij}} + \sum_{A=1}^{M}\sum_{B>A}^{M}\frac{Z_A Z_B}{r_{AB}}. \quad (2.2)$$

In equation 2.2 the first two terms describe the kinetic energy of the electrons and nuclei. The third term represents the attractive electrostatic interaction between the nuclei and the electrons. The fourth and fifth terms represent the arepulsive potential due to the electron-electron and nucleus-nucleus interactions respectively.

Nuclei being much heavier than electrons, move much slower. Hence, the electrons can be considered to be moving in a field of fixed nuclei. This is the Born-Oppenheimer approximation which makes the nuclear kinetic energy insignificant and renders the nuclear potential energy to be a constant. The electronic Hamiltonian then reduces to:

$$\hat{H}_{elec} = -\frac{1}{2} \sum_{i=1}^{N} \nabla_i^2 - \sum_{i=1}^{N} \sum_{A=1}^{M} \frac{Z_A}{r_{iA}} + \sum_{i=1}^{N} \sum_{j>i}^{N} \frac{1}{r_{ij}}, \qquad (2.3)$$

which gives us the reduced Schrödinger equation:

$$\hat{H}_{elec} \psi_{elec} = E_{elec} \psi_{elec}. \qquad (2.4)$$

This complicated many-particle equation is not separable into simpler single-particle equations because of the interaction terms (last two terms in equation 2.3). After the Schrödinger equation was put forth and validated spectacularly for systems like H and H_2, Dirac is famously said to have proclaimed, as mentioned by Kohn [13] - 'chemistry had come to an end - its content was entirely contained in that powerful equation. Too bad, he is said to have added, that in almost all cases, this equation was far too complex to allow solution'. Since then, much progress has been made in finding approximate solutions to the Schrödinger equation for the many-electron problem.

Density functional Theory (DFT) is an alternative approach to the theory of electronic structure, in which the electron density distribution $n(r)$ plays an important role. The Thomas-Fermi theory arguably was the first primitive form of DFT put forth by Thomas [14] and Fermi [15] in 1927. DFT, as it is known today, was reported over the course of two works -Hohenberg and Kohn in 1964[16] and Kohn-Sham in 1965 [17] and is based on the two Hohenberg - Kohn (H-K) theorems. The first Hohenberg-Kohn theorem demonstrates that the electron density uniquely determines the Hamiltonian operator and thus all the properties of the system. The second H-K theorem defines a ground state energy functional and proves that it delivers the lowest energy if and only if the input density is the true ground state

density.

This electron density is defined as the integral over the spin co-ordinates of all electrons and over all but one of the spatial variables:

$$\rho(\vec{r}) = N \int ... \int |\psi(\vec{x}_1, \vec{x}_2, \vec{x}_3...\vec{x}_N)|^2 ds_1 d\vec{x}_2 .... d\vec{x}_N \tag{2.5}$$

When reformulated in terms of the electron density, the Schrödinger equation reduces to the Kohn-Sham equation:

$$-\left[\frac{1}{2}\nabla^2 + V(\vec{r}) + V_H(\vec{r}) + V_{XC}(\vec{r})\right] \psi_i(r) = \epsilon_i \psi_i \tag{2.6}$$

Here, $V(r)$ accounts for the interaction between the nuclei and the electrons, V_H is the Coulombic interaction between electron at position x_i and the average charge distribution of another electron in spin orbital ψ_j. This term is the Hartree potential. This potential is non-local and it depends on the spin orbitals. Thus, these equations must be solved self-consistently. V_{XC} is the exchange-correlation potential which includes the many-particle interactions. This V_{XC} is the holy grail of DFT. It is defined as the functional derivative of E_{XC} with respect to the electron density $(\rho(\vec{r}))$, i.e., $V_{XC} = \frac{\delta E_{XC}}{\delta \rho(\vec{r})}$. If the exact forms of E_{XC} and V_{XC} were known, the Kohn-Sham equations would lead to the exact energy. However, the exact functionals for exchange and correlation are not known except for the case of the free electron gas. A number of approximations exist to estimate these exchange - correlation potentials. The local density approximation (LDA) [18] as the name suggests assumes that the exchange energy per particle in each spatial point depends only on the local density. The generalized gradient approximation (GGA) [19] uses the local electron density as well as the local gradient in the electron density.

In this work, we use the Vienna *ab initio* simulation package (VASP) [20, 21, 22, 23] to perform the *ab initio* calculations. VASP uses plane-wave (PW) basis sets and uses the Hellmann-Feynman [24, 25] theorem to calculate forces. The interaction between ions and electrons is described by the projector augmented-wave (PAW) method [26].

2.2   Lattice Dynamics Calculations

Martensitic transformations are often found to occur at a critical valence electron concentration (e/a) and concommitant vibrational anomalies are of importance. Lattice dynamics calculations involve the determination of the constrained free energy of a system in the neighborhood of an equilibrium conguration ϕ, assuming that the system is to be found most of the time in the vicinity of a local energy minimum where a harmonic approximation to the energy surface may be made accurately. Vibrational properties are calculated by using the reaction forces resulting from imposed atomic displacements. The most important part of the calculations involve the calculation of the force constants. Force constants may be calculated in three ways: analytic calculations, supercell calculations and linear response calculations. In simple cases when a direct calculation of the second derivatives of the energy with respect to atomic displacements is allowable, analytic calculations are possible. In the supercell method, the atoms are slightly perturbed from their equilibrium positions and the reaction forces are calculated. Equating the calculated forces to the predicted forces from the harmonic model results in a set of linear constraints which may be used to determine the force constants. In the supercell method [27, 28], the positions of the atoms are slightly perturbed away from their equilibrium position and the reaction forces are calculated. A set of linear constraints are obtained by equating the calculated forces to the forces predicted from the harmonic model. From

9

these, the unknown force constants are determined. In the linear response method [29, 30] second-order change in the electronic energy resulting from the perturbations are used to directly evaluate the dynamical materix associated with the harmonic system. The eigenvalues of this matrix give the frequencies of the normal modes of oscillations, which are then used to calculate the vibrational properties. Phonon vibrational density of states (PVDOS) calculations were carried out using VASP in conjunction with the fitfc module of the ATAT package [31].A full relaxation of the structure is first carried out. Then the structure is subjected to perturbations and the vibrational properties are calculated by fitting a spring model to reaction forces resulting from imposed atomic displacements.

2.2.1   Calculation of elastic constants

The elastic constants were calculated by imposing a set of strains [32, 33, 34, 35, 36], $\epsilon = (\epsilon_1, \epsilon_2, \epsilon_3, \epsilon_4, \epsilon_5, \epsilon_6)$ on the crystal structure. The stresses (σ_i) resulting from the change in energy due to the deformation are calculated. By application of Hooke's Law $\sigma_i = C_{ij}\epsilon_j$, the stiffness tensor C_{ij} may be computed. The Bulk Modulus (B) is calculated according to [36]:

$$B = \frac{2}{9}\left(C_{11} + C_{12} + 2C_{13} + \frac{C_{33}}{2}\right) \tag{2.7}$$

The shear modulus is calculated using the Voight approximation[36]:

$$G = \frac{1}{15}\left(2C_{11} + C_{33} - C_{12} - 2C_{13}+\right) + \frac{1}{5}\left(2C_{44} + \frac{1}{2}(C_{11} - C_{12})\right) \tag{2.8}$$

While Young's modulus is computed by[36]:

$$E = \frac{9BG}{3B + G} \tag{2.9}$$

and Poisson's ratio may be calculated as:

$$\nu = \frac{E}{2G} - 1 \tag{2.10}$$

2.3 String Algorithm for calculation of Minimum Energy Path (MEP)

Calculating the energy landscape of a system with respect to the phenomenon of interest (for example the martensitic transformation in SMAs) allows us to see the local and global minima and maxima which lend greater insight into the transformation. The question that arises next is which path the transformation will take to transition from a local minimum to another local minimum. The path taken by the transformation is the minimum energy path (MEP) or the path of least resistance. These MEPs can be mathematically defined as the paths in the configuration space along which the potential force is parallel to the path at every point. The MEPs can be then used to identify the relevant saddle points which act as the bottlenecks for a particular barrier-crossing event as well as the energy barriers associated with the transformation. These energy barriers in turn lend an insight into the energy required for the transformations to occur. A number of computational methods exist to determine the MEP given an energy landscape. Well known ones include the zero-temperature string method [37] and the Nudged Elastic Band (NEB) [38] method. In this work we use the zero-temperature string method to determine the MEPs over the martensitic transformation energy landscapes. The basic idea behind this method is to find the MEP by evolving a curve connecting the initial and final configurations, under the energy field. Only the normal component of the first derivative matters since the tangential component only varies the positions of points along the curve, causing a change in parameterization of the curve without any change in the curve itself. For more details the reader may refer to [39].

2.4   Minima Hopping Algorithm to predict crystal structures

Minima hopping [40] is a technique that may be used to ind the global minimum of complicated condensed matter systems. The algorithm works so as explore the low energy areas of a configurational space as fast as possible while limiting the number of revisits to known regions. It exploits the Bell-Evans-Polyani principle [41], i.e. it moves from one minimum to the next by crossing low barriers which significantly increases the probability of hopping into a low energy local minimum. To put this another way it operates on the principle that crossing from the current basin over a low energy barrier into a new basin is more likely to yield a low energy local minimum than if one overcomes a high barrier. For further details, one may refer to [40]

3. INVESTIGATION OF THE ENERGETICS OF STRUCTURAL TRANSFORMATIONS IN CO-BASED BINARY ALLOYS

3.1 Introduction

Pure cobalt shows a non-thermoelastic reversible martensitic transformation from a parent face-centered (f.c.c - γ) phase to a hexagonal close-packed (h.c.p - ϵ) phase at $\simeq$ 695K [42]. The transformation is accompanied by small changes in enthalpy ($\Delta h = 473 \mathrm{J\,mol^{-1}}$) and volume ($\Delta V/V = 3.3 \times 10^{-3}$) and a sharp singularity of the specific heat, attesting to it being a first order transformation [43]. The system has a thermal hysteresis associated with it ($\approx$ 100K) which is quite high when compared with conventional thermoelastic SMAs. A number of factors affect the transformation temperature, such as grain size, purity, external stresses and alloying [42]. Binary alloying drastically affects the transformation temperature in these alloys, as zirconium and molybdenum cause a reduction in the martensitic start temperature (M_s) with increased alloying while germanium and silicon additions result in an increase in M_s. Addition of aluminium or nickel do not affect the transformation temperature significantly [42, 44].

In 2003, Omori et al.[44] showed that the addition of aluminium to cobalt promotes $L1_2$ ordering and thereby improves the reversibility of the transformation. The solubility of Al in Co is $\approx$ 16% and the alloying does not reduce the ductility of the material. Consequently, Co - Al is a potential high temperature SMA (HTSMA) with high thermal stability.

A number of attempts have been made to model the f.c.c-h.c.p phase transformation. The majority of these models describe the transition in terms of nucleation and growth processes and the propagation of partial dislocations [45, 46, 47]. The other

class of models are phenomenological models based on shearing mechanisms formulated by the decomposition of the distortion into two configuration co-ordinates. The Shoji - Nishiyama [3] mechanism was the earliest such model which described a way of continuously distorting the f.c.c structure into a h.c.p structure using the simple hexagonal (s.h) reference structure, specifically for the transformation in cobalt alloys. More recently, Wentzcovitch et al. [48] proposed a parametric model to describe this transformation using an orthorhombic reference structure. As mentioned above, the martensitic transformation in cobalt is a displacive transformation accomplished by the cooperative movement of atoms while maintaining the primary co-ordination and thereby lends itself well to analysis using parametric models. In this work, the martensitic transformations in Co-based binary alloys are investigated using the two phenomenological models described above using *ab initio* methods within a DFT framework with a view to assessing the effect of alloying on the energetics of the transformation. Kibey at al[49] use a similar process to model the $B2 - B19'$ transformation in Ni-Ti.

These models yield the energy landscapes for the transformations given the initial and final structures. For transformations with relatively smooth energy surfaces, the most probable pathways are the minimum energy paths (MEP). Minimum energy paths have physical significance in the low temperature behavior of a system as they give insight into the energy barrier involved in a thermally activated event (phase transformation) without any inputs about the width of the channel near the saddle point or other effects due to entropy. The energy surfaces calculated in this work are a result of ground state calculations and hence are sufficiently smooth to bear relevance for MEP calculations. At high temperature, thermal fluctuations cause the energy surface to lose smoothness and multiple energy peaks of the order of kBT make the concept of the MEP irrelevant. However at high temperatures, the MEP will still

14

correspond to the path with the maximum likelihood. Thus the problem reduces to obtaining the MEP over a energy surface when the initial and final states are known. The techniques used for such scenarios include the string method [50, 51] and the nudged elastic band(NEB) [38] methods. In this work we use the string method as implemented by Samanta et al. [51] to determine the MEP for the transformations.

The objective of this work is to build a framework to assess the viability of martensitic transformations in Co-based binary alloys from an energetics point of view, to investigate the effect of Al alloying on the transformation, and finally, to extend the framework to allow investigations on other binary Co-based alloys. Additionally, the framework may be used to study other SMAs which show similar transformations.

The organization of this article is as follows. In Section 3.2 we debate the applicability of the Bain transition mechanism in the case of Co-based alloys and show the energetics of the Bain path in the Co - Al system. In Section 3.3 the phenomenological models for the f.c.c to h.c.p transformation are discussed and applied to the binary Co - Al, Co-Si, and Co-Fe binary alloys by extending the ideas presented in [48, 52] . In Section 3.4 the minimum energy paths for the transformations are realized using a steepest descent algorithm and the results are compared with experimental data. An attempt is made to provide a theoretical basis for the minimum energy paths obtained. Finally, in Section 3.5 we summarize our results and conclude by delineating the characteristics of the martensitic transformation in Co-based alloys.

3.2   f.c.c - b.c.c transformation

Cobalt is the only element displaying a f.c.c-h.c.p transition which does not possess a disordered body centered (b.c.c) phase in it's phase diagram. In elements which do possess the b.c.c phase, the f.c.c and h.c.p structures can be attained from the parent bcc structure via the Bain [53] and Burgers [54] transformations. The
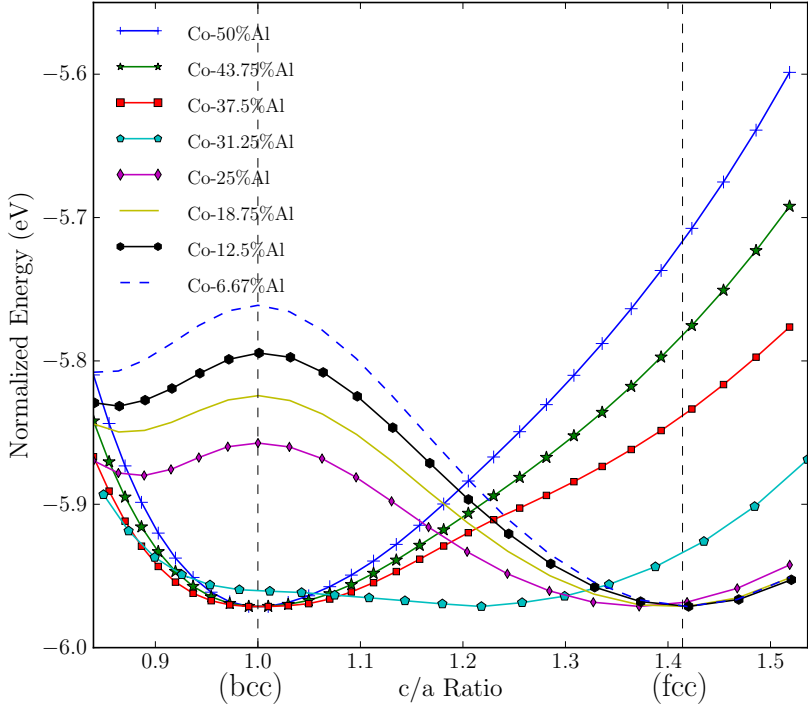
Figure 3.1: Bain path in Co - Al for alloying up to 50% Al

Co - Al phase diagram however, shows a bcc phase at compositions greater than around 25 % Al. To validate the use of these distortion models, the phase stability of competing phases was studied by carrying out Bain path calculations for the Co - Al system for up to Co-50 % Al as shown in Figure 3.1.

It is seen that the Co - Al system shows a minima at a c/a ratio of ≈ 1.43 up to Co-25% Al. Beyond 25% Al there is a sharp shift in the stability and the bcc structure (c/a = 1) is stabilized for increasing amounts of Al, which agrees with the Co - Al phase diagram in that this system is dominated by a B2 - ordered phase close to the 1:1 stoichiometry. While the Bain path is not relevant to the problem at hand, the fact that it's composition dependence closely mirrors the expected topology of the binary phase diagram constitutes an indirect validation of the accuracy of the

calculations.

3.3   f.c.c - h.c.p transformation

It is well established experimentally that Co - Al alloys show a f.c.c - h.c.p transformation with a good shape memory effect for Al $> 10\%$ [44]. On an atomic level, the martensitic transformation is realized by a combination of finite displacements (shuffles) along various directions. However, the energy path associated with this transformation has not been previously examined to the best of the authors knowledge. This work explores the energy surface associated with the f.c.c - h.c.p transformation in Co - Al via two mechanisms mentioned in section 3.1: the conventional Shoji- Nishiyama path [3] and the recent mechanism presented by Wentzcovitch et. al. [48]. The energy lansdscape for the f.c.c -h.c.p transformation using both models for the sample case of pure aluminium is shown in Figure 3.2.

3.3.1   Shoji-Nishiyama (SN) path for the f.c.c-h.c.p transformation in Co - Al

The SN path models a continuous distortion of the parent f.c.c phase into the h.c.p phase which can be visualized by a decomposition into two configurational co-ordinates as proposed by Folkins and Walker [52]; one accounting for the shearing of the crystal and the other describing the relative sinusoidal displacements of atomic planes. The planar correspondence is given by: $(111)_{fcc} \parallel (0001)_{hcp}$, $[11\bar{2}]_{fcc} \parallel [1\bar{1}00]_{hcp}$, or $[1\bar{1}0]_{fcc} \parallel [11\bar{2}0]_{hcp}$. This transformation occurs by shifting every other (111) f.c.c plane by $(a/6)[11\bar{2}]$. The parameterization of this transformation as formulated by Folkins and Walker is used for the calculations. The formulation uses the simple hexagonal (s.h) structure as a reference structure. The f.c.c structure is then generated from the s.h structure by a shear along the $\hat{x}$ direction. The h.c.p structure is derived from the s.h structure by an alternating modulation along the $\hat{x}$ direction. For an atom with position vector $r = (x, y, z)$, it's displacement

17

(a)   (b)
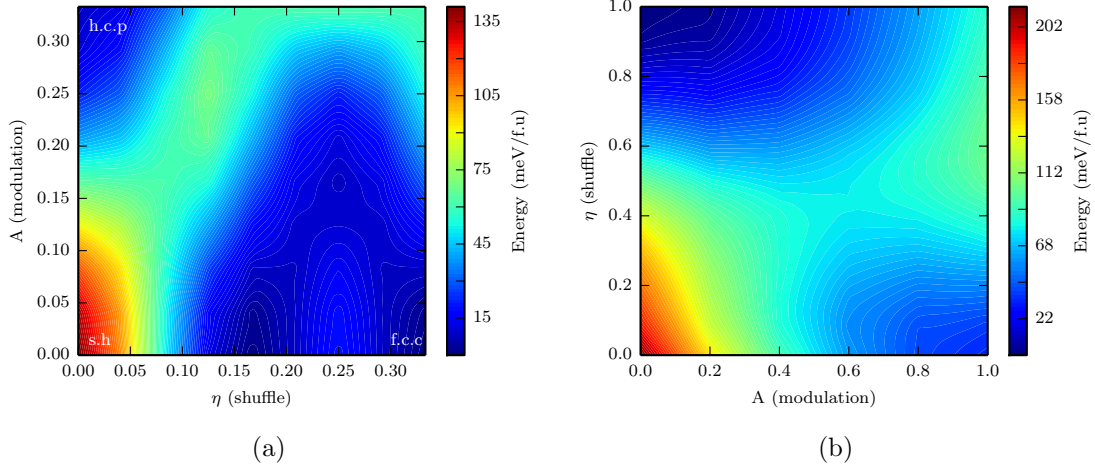
Figure 3.2: F.c.c -h.c.p energy contours for pure aluminium.(a) SN mechanism. (0,0) corresponds to the s.h reference structure, $(0, \frac{1}{3})$ corresponds to the h.c.p structure while $(\frac{1}{3}, 0)$ indicates the f.c.c structure. (b) WL mechanism. (0,1) refers to the f.c.c structure while (1,0) describes the h.c.p structure.

is then given by equation 3.1:

$$u(A, \eta; r) = \eta \frac{3}{\sqrt{2}} z \hat{x} + A \frac{\sqrt{3}}{2} a \cos(Q.r) \hat{x} \tag{3.1}$$

with $Q = (\frac{\pi}{c})\hat{z}$. The η term on the right hand side of the equation denotes the shear.

It describes the lateral shearing of each hexagonal plane by $\eta \frac{3}{\sqrt{2}} z$. The second term

describes the modulation associated with the h.c.p structure. For further details

regarding this formulation, refer to [52]. As seen in Figure 3.2a; (0,0) corresponds

to the s.h reference structure, $(0, \frac{1}{3})$ corresponds to the h.c.p structure while $(\frac{1}{3}, 0)$

indicates the f.c.c structure.

3.3.2   *Wentzkovitch-Lam (WL) path for the f.c.c - h.c.p transformation in Co - Al*

The alternate model proposed by Wentzkovitch [48] assumes a correspondence

between $(001)_{fcc}$ and $(0001)_{hcp}$ planes. This is achieved by the simultaneous oc-

18

currence of four strains [48]: (i) shear in opposite directions of the A and B layers along $[100]_{fcc}$ or $[010]_{fcc}$,(ii) a macroscopic strain along $[100]_{fcc}$ or $[010]_{fcc}$, (iii) another macroscopic strain along $[001]_{fcc}$, and (iv) a compressive strain along $[010]_{fcc}$ or $[100]_{fcc}$.

Atomic Displacement of an atom at r(x,y,z) within this formulation is given by equation 3.2:

$$u(A, \epsilon_x, \epsilon_y, \epsilon_z; r) = \epsilon_x x \hat{x} + \epsilon_y y \hat{y} + A(1 + \epsilon_y)\frac{a}{\sqrt{2}}cos(Q.r)\hat{y} + \epsilon_z z \hat{z} \qquad (3.2)$$

where $Q = (2\pi/L)\hat{z}$ and $L = \sqrt{2}a$. $(1+\epsilon_x)+(1+\epsilon_y)+(1+\epsilon_z) = 1$ for both structures which implies a volume invariance. For more details please refer to [48]. As seen in Figure 3.2b, (1,0) corresponds to the h.c.p structure and (0,1) to the f.c.c structure.

The minimum energy path (MEP) for the SN and WL mechanisms were then calculated using the modified string method[51], and are indicated in Figure 3.3.

3.4   Results and Discussion

Calculations presented in this work were performed within the framework of Density Functional Theory, as implemented in the Vienna *ab initio* simulation package (VASP), applying the generalized gradient approximation (GGA) using the Perdew-Wang 1991 (PW91) functional [55]. The electronic configurations of the appropriate elements were realized using the projector augmented-wave (PAW) pseudo-potentials formalism [26]. Brillouin zone integrations were performed using a Monkhorst-Pack mesh [56] with atleast 5000 k-points per reciprocal atom. Full relaxations were realized by using the Methfessel-Paxton smearing method of order one [57] and self-consistent static calculations were carried out with the tetrahedron smearing method with Blöchl corrections [58]. A cutoff energy of 350 eV was used for all the calculations and spin polarizations were accounted for as well. The f.c.c - h.c.p transforma-
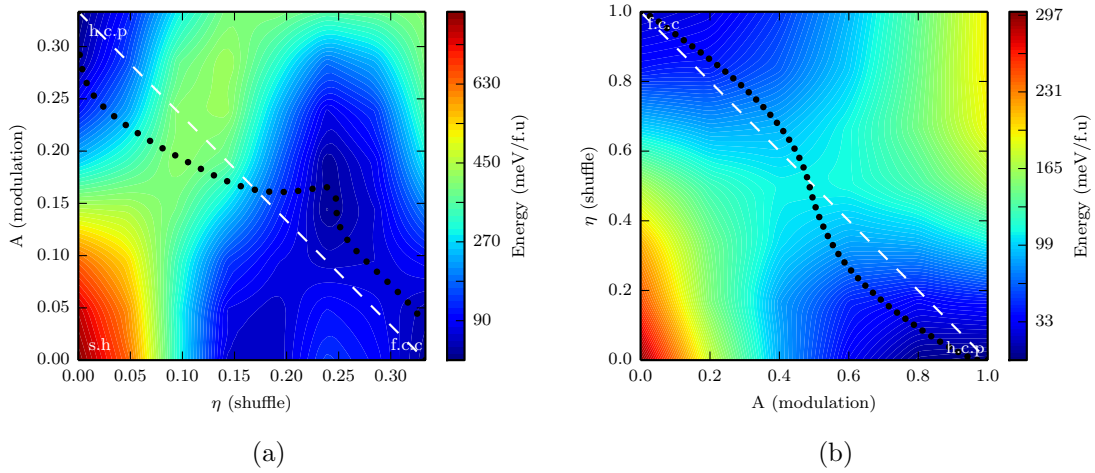
Figure 3.3: Calculated MEP using the modified string method for pure cobalt. (a) SN mechanism. The dashed line indicates the initial straight line path while the line with circular markers indicates the final optimized MEP. b) WL mechanism. The dashed line indicates the initial straight line path while the solid line with circular markers indicates the final optimized MEP.

tion was modeled using the Wentzcovitch-Lam (WL) and the Shoji-Nishiyama (SN) mechanisms for the Co - Al, Co-Fe and Co-Si systems. The results are presented below.

This section shows the results obtained for the f.c.c. - h.c.p transformation paths using the WL and SN models. Calculations have been carried out for the Co - Al, Co-Fe, and Co-Si systems. For both Al and Fe, experiments have shown that the martensitic transformation temperature of cobalt is expected to decrease with increased alloying. The addition of Si shows the opposite effect, the martensitic tranformation temperature increases with increased alloying [59]. Figure 3.4a shows the MEP profiles for varying compositions of Co - Al and Figure 3.5a shows the trend observed in the energy barrier for the transformation for varying compositions of Co - Al for the Shoji-Nishiyama model. The SN model shows a contrasting trend. We see an increase in the energy barrier (which indicates an increase in M_s) with increasing
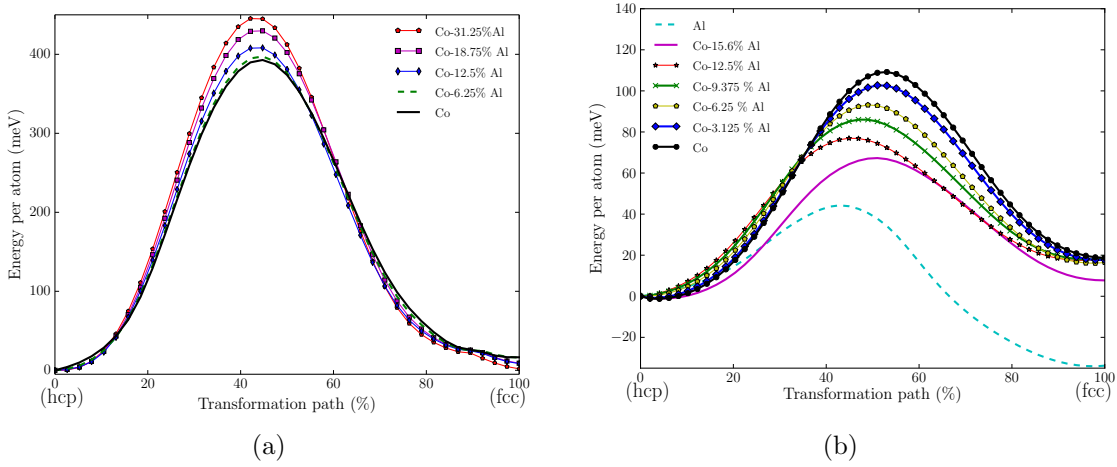
Figure 3.4: MEP profile for various compositions of Co - Al for the (a) SN, and (b) WL mechanisms

amounts of Al which is opposite to what is known experimentally. Additionally, the energy barriers calculated are also more than three times higher than that for the WL model.
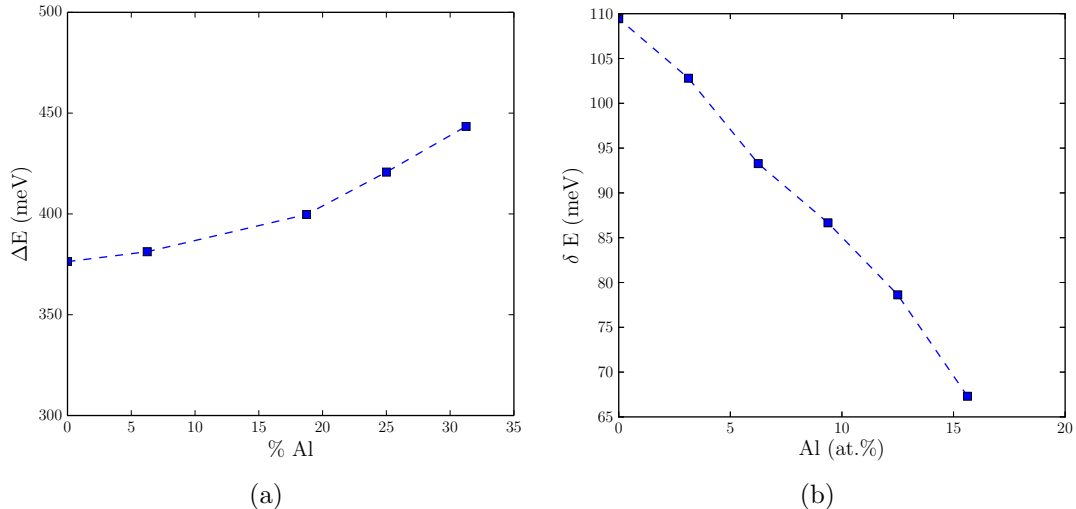
Figure 3.5: Energy barrier trend as a function of Al % for the (a) SN, and (b) WL mechanisms

Figure 3.4b shows the MEP profiles for varying compositions of Co - Al and Figure 3.5b shows the trend observed in the energy barrier for the transformation for varying compositions of Co - Al using the WL model. We see a reduction in the energy barrier (which indicates a lowering of M_s) for increasing amounts of Al, which is corroborated by experimental works [44] which indicate a lowering of the M_s with addition of aluminium. This trend stays the same throughout the range of composition for which calculations were carried out.

A SN model with zero transformation deformation may also be formulated by considering a combination of deformations in the three equivalent shear directions [3]. Planar shifts of $(a/6)[\bar{2}11]$, $(a/6)[1\bar{2}1]$ on the (111) f.c.c plane are equivalent to $(a/6)[11\bar{2}]$. Each of these shifts causes a total shear of 19.5°. If these three variants are stacked with equal thickness the resultant deformation shear will reduce to zero, i.e they will cancel each other in the bulk cell. This will mean a small resultant shear for the martensitic transformation and may result in an easier transformation. This model was also implemented for comparison and calculations were carried out for the Co - Al system. Figure 3.6a shows the MEP profiles for varying compositions of Co - Al and Figure 3.6b shows the trend observed in the energy barrier for the transformation for varying compositions of Co - Al for the modified zero transformation deformation Shoji-Nishiyama model. Comparing figures 3.4a and 3.6a, it is seen that while there is a reduction in the absolute values of the energy barrier for the transformation compared to the simple SN model, it is still much higher than for the WL model. Additionally, in figure 3.6b we still see an increase in the energy barrier with addition of Al, contrary to experiments. Consequently, we do not use the zero deformation shear model for any further analysis.

Figure 3.7a shows the MEP profiles for varying compositions of Co-Fe and Figure 3.8a shows the trend observed in the energy barrier for the transformation for varying
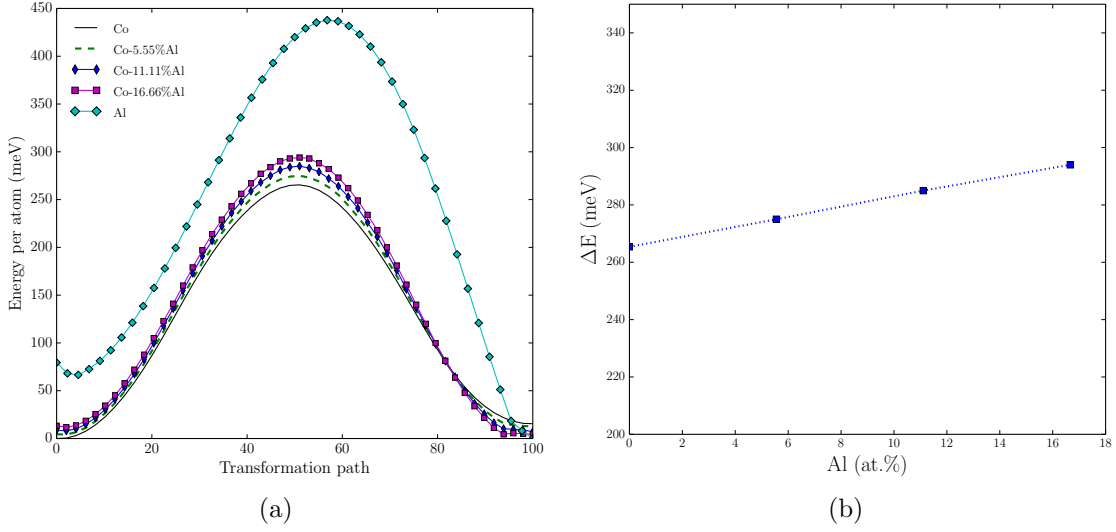
Figure 3.6: (a) MEP profile for various compositions of Co - Al, and (b) Energy barrier trend as a function of Al % for the modified zero transformation shear SN mechanism
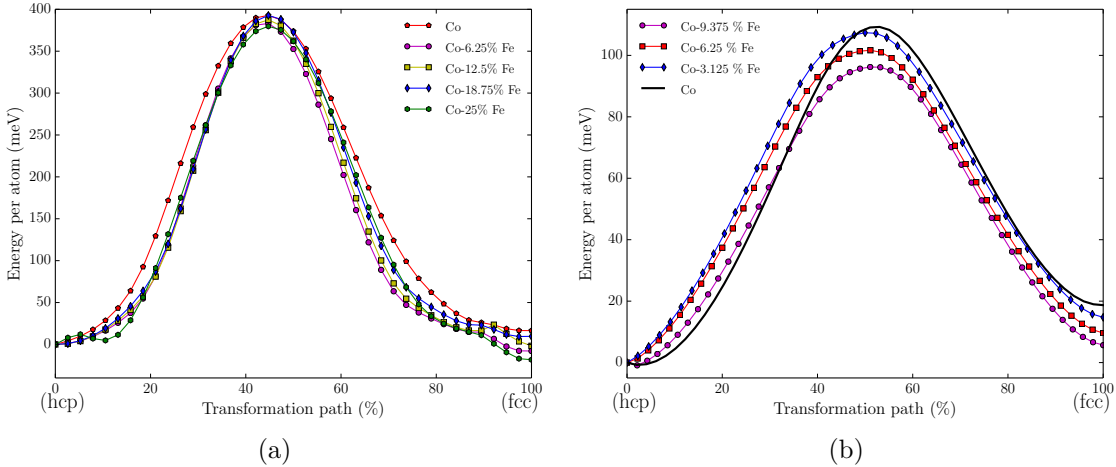
Figure 3.7: MEP profile for various compositions of Co-Fe for the (a) SN, and (b) WL mechanisms

compositions of Co-Fe for the Shoji-Nishiyama model. Figure 3.7b shows the MEP profiles for varying compositions of Co-Fe and Figure 3.8b shows the trend observed
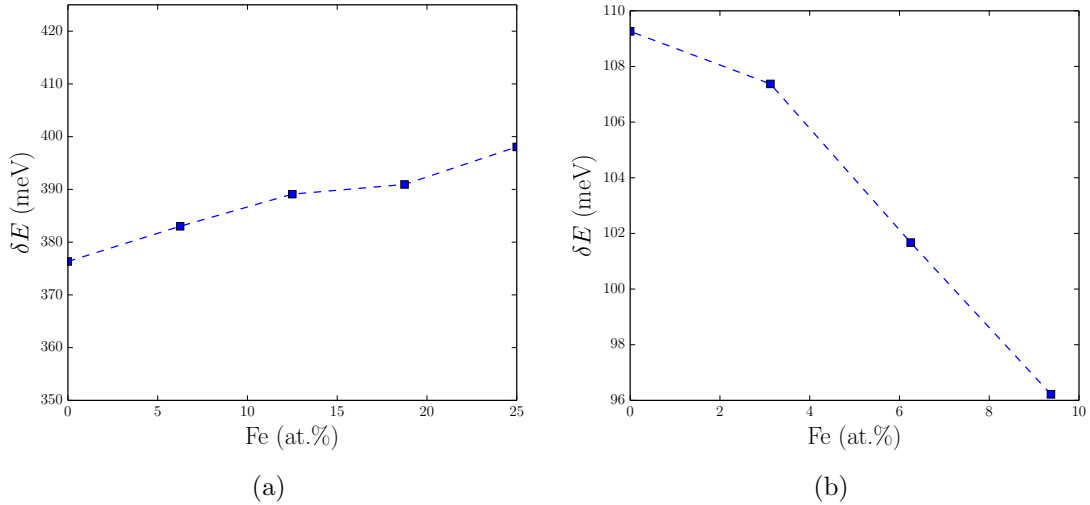
Figure 3.8: Energy barrier trend as a function of Fe % for the (a) SN, and (b) WL mechanisms

in the energy barrier for the transformation for varying compositions of Co-Fe using the WL model. In the Co-Fe system , the SN model shows an increase in the energy barrier while the WL model shows a reduction in the energy barrier (which indicates a lowering of M_s) for increasing amounts of Al. Thus, only the WL model agrees with experimental data [59].

Figure 3.9a shows the MEP profiles for varying compositions of Co-Si and Figure 3.10a shows the trend observed in the energy barrier for the transformation for varying compositions of Co-Si for the Shoji-Nishiyama model. Figure 3.9b shows the MEP profiles for varying compositions of Co-Si and Figure 3.10b shows the trend observed in the energy barrier for the transformation for varying compositions of Co-Si using the WL model. In the Co-Si system , both models show a reduction in the energy barrier (which indicates a lowering of M_s) for increasing amounts of Si, which is contrary to what may be expected from experiments[59].

Thus it is seen that the WL model predictions agree with experiments for the
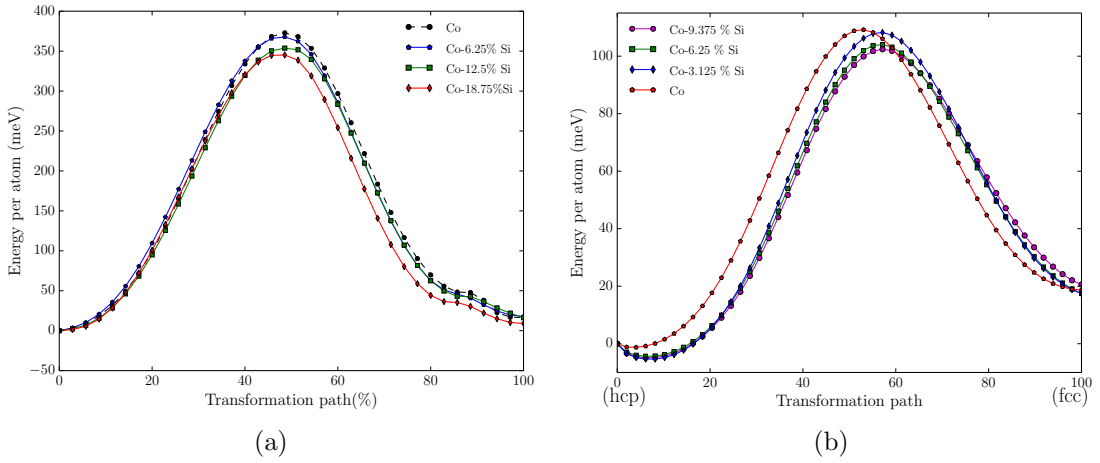
Figure 3.9: MEP profile for various compositions of Co-Si for the (a) SN, and (b) WL mechanisms
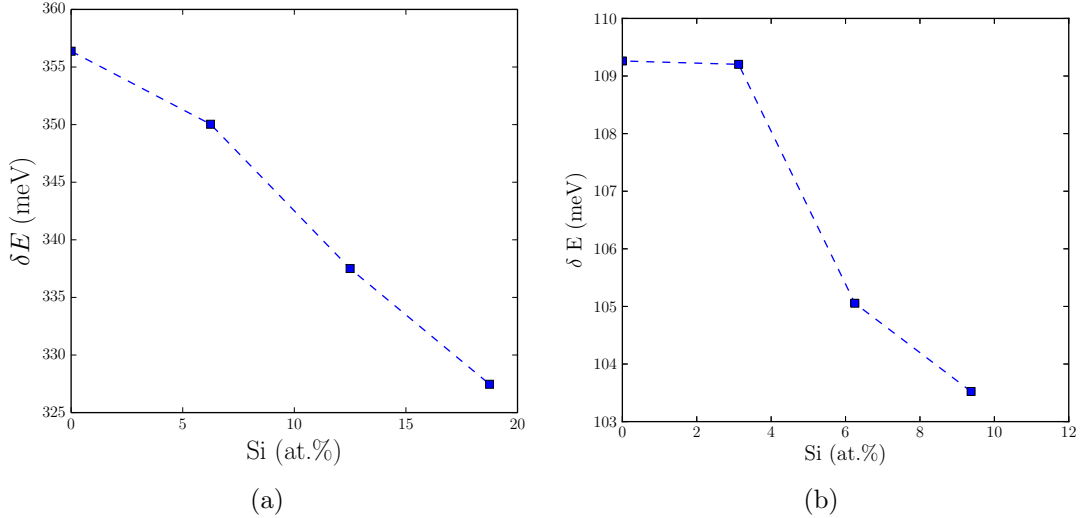
Figure 3.10: Energy barrier trend as a function of Si % for the (a) SN, and (b) WL mechanisms

Co - Al and the Co-Fe systems. Both mechanisms fail to explain the trends seen in Co-Si. It may therefore be possible, that the underlying energetics of the Co-Si system are far removed fom those of the Co - Al and Co-Fe systems. We propose

25

that the martensitic transformation in Co - Al and Co-Fe may be explained by the Wentzcovitch -Lam model.

While noting the MEP indicated by both mechanisms we see that the the MEP always passes through an intermediate structure and does not show the slightest tendency to deviate from the intermediate structure. This can be explained on the basis of space group symmetry. A space group is a set of symmetry elements which always fulfill certain conditions according to the mathematics of the particular group. If G_n is a space group consisting of certain n symmetry elements and G_m is another space group with m symmetry elements such that $m \subseteq n$,then G_m is the sub-group of G_n while G_n is the super-group of G_m. The martensitic transformation under consideration, is a barrier crossing event. The transformation occurs from the f.c.c structure to the h.c.p structure. F.c.c is a high symmetry structure with a space group of 225 while h.c.p is a comparatively low symmetry structure (space group 194). Thus the transformation involves a reduction of symmetry. Reduction of symmetry happens through intermediate common subgroup structures-transition states. This makes it necessary to used an optimization method to calculate the MEP. Not using a specific MEP method makes us overlook the transition states which reflect the true mechanism of transformation. For f.c.c and h.c.p we see the common subgroup with the highest symmetry is the *Cmcm* orthorhombic structure (space group:63). On examining the structure of the intermediate state indicated by the MEP, it is seen that it is the *Cmcm* structure with a space group of 63.

3.5 Summary and Conclusion

The present work deals with the application of displacive transformation models to Co-based potential shape memory alloys. The f.c.c-b.c.c and f.c.c -h.c.p transformations have been modeled for the Co - Al and the Co - Al, Co-Fe, Co-Si systems

respectively. The Bain path calculations for Co - Al showed an energy minimum at a tetragonal structure upto 25 % Al and indicated a theoretical possibility for the f.c.c - b.c.c transformation in Co - Al. The lack of a b.c.c phase in the cobalt phase diagram however, prohibits the expectation of this transformation in this system. Two varied parameterized models were used to model the f.c.c - h.c.p structural transformation for three Co-based SMAs. The Wentzcovitch - Lam model predictions agree with experiments for the Co - Al and the Co-Fe systems. The Shoji-Nishiyama mechanism calculations agree with experiments for the Co-Fe system. Both mechanisms fail to explain the trends seen in Co-Si. It may therefore be possible, that the underlying energetics of the Co-Si system are far removed from those of the Co - Al and Co-Fe systems. We propose that the martensitic transformation in Co - Al and Co-Fe may be explained by the Wentzcovitch - Lam model. The intermediate structures obtained across both models for all the systems conform to the common symmetry subgroup theory

4. STABILITY ANALYSIS OF THE MARTENSITIC PHASE TRANSFORMATION IN CO₂NIGA HEUSLER ALLOY*

Over the last few decades, experimental and theoretical research into shape memory alloys (SMAs) has gained momentum due to the need for high - temperature multifunctional materials. Current applications are restricted to below 100°C for $Ni - Ti$-based and Cu-based alloys which have transformation temperatures in that range. To be able to realize the advantages offered by these multi-functional materials in the automotive, aerospace and heavy - machinery industries, there is a requirement for SMAs with much higher transformation temperatures. CoNiGa is one such promising SMA which is the object of much interest due to its potential as a magnetic SMA with a thermoelastic transition in the ferromagnetic state [60]. Cobalt has a large magnetic moment which ensures a high Curie temperature. The CoNiGa alloy is sufficiently ductile, exhibits the shape memory effect (SME), and has excellent super - elastic properties [61]. Additionally, it shows martensitic start (M_s) temperatures up to 250°C [62]. The CoNiGa alloy with a stoichiometric Heusler - type composition (Co_2NiGa) is a primary candidate for applications requiring ferromagnetic shape memory alloys[63, 64, 65, 66].

Heusler alloys may be defined as ternary inter-metallic compounds with a stoichiometric composition X_2YZ, with the $L2_1$ crystal symmetry. The $L2_1$ unit cell belongs to the space group $Fm\bar{3}m$ and the whole crystal shows only tetrahedral symmetry. X and Y are transition metals while Z is usually a covalently bonding

group III-V element. The Heusler structure is bcc-like as it can be formed from the ordered combination of two binary B2 compounds XY and XZ with CsCl structure [67]. Austenitic Co_2NiGa exhibits the Heusler $L2_1$ structure (space group $Fm\bar{3}m$) with two inter - penetrating binary B2 compounds CoNi and CoGa with a CsCl structure. The related inverse Heusler structure (CoNi)CoGa can be described as one in which the Co sub - lattice is occupied by the Ni atom, while the displaced Co atoms sit on the Ni sites. DFT calculations have shown that the inverse Heusler structure competes with the conventional Heusler structure in some cases [68].

In the Co_2NiGa system, there is a martensitic transformation from the ordered cubic $L2_1$ to the non - modulated tetragonal $L1_0$ (AuCu, space group $P4/mmm$, 123) phase. Modulated martensites which are seen in Ni(Mn,Fe)Ga Heusler alloys, have not been observed in the CoNiGa system [69, 70]. The $L2_1$ to $L1_0$ transformation can be described as a tetragonal distortion of the cubic austenitic phase. If one assumes that the transformation occurs with minimal volume change, then it can be described through a Bain path, which essentially transforms a bcc structure into a fcc variant as the c/a ratio of the lattice goes from 1 to $\sqrt{2}$. In this transformation,$c/a = 1$ corresponds to the $L2_1$ phase, while the minimum at $c/a = \sqrt{2}$ corresponds to the low - symmetry, low - energy martensite $L1_0$ with structural symmetry.

Along with the Bain mechanism, the body centered cubic (bcc) - hexagonal close packed (h.c.p) transformation is the most commonly observed reconstructive phase transformation in simple crystals. It is found in about 20 elements [71]. The mechanism used to describe this transformation is the Burgers path [72], first proposed for the $\beta - \alpha$ transformation in Zr. When applied to the CoNiGa system, surprisingly, the Burgers path is seen to be a barrier - less transformation that reaches a minimum value at distortions resulting from shuffles and shears. This minimum corresponds to a low-energy martensitic structure with orthorhombic symmetry (space group 59),

referred to as the O structure henceforth which is more stable (has a lower energy) than the conventional martensitic $L1_0$ structure. The O phase has yet to be reported in the literature and its absence in experiments cannot be merely explained away using kinetic barrier arguments as the transformation clearly can go forward in a monotonic way, at least under ground state—i.e., low - temperature conditions.

In an effort to explain this unprecedented O phase, an extensive investigation was carried out to provide insight into the phenomenon by exploring the energy landscape around the cubic Co_2NiGa composition. A structural search by using the minima hopping method[40] was carried out to explore the energy landscape surrounding the conventional martensitic $L1_0$ structure. These calculations predicted a number of structures with monoclinic, tetragonal, and orthorhombic symmetries with energies much lower than the $L1_0$ structure as well as the O phase, with energy differences much larger than typical computational errors within the chosen approximations. Various high-throughput databases such as the Materials Project [73], the Open Quantum Materials Database (OQMD) [74], and Automatic Flow for Materials Discovery (AFLOW) [75] did not yield any of the structures predicted by the minima hopping method (MHM) or the Burgers calculations. This may be attributed to the lesser number of known structures for ternary phases, making predictions based on data mining very difficult beyond binary systems or that those methods have been not used in particular for this type of compound.

Even with the extensive energy landscape exploration, the question as to why the Co-Ni-Ga system undergoes a martensitic transformation to the $L1_0$ phase,- while other lower energy structures, specifically the O phase which may be accessed via the Burgers path, exist still remains to be answered. The question may be addressed in either one of three ways: (i) DFT within a set of given approximations is inadequate to capture the energetics of the transformations in the Co-Ni-Ga system;

(ii) experiments have so far been unable to isolate the true martensitic ground state of the system; (iii) the problem may be resolved by invoking phase competition/phase selection at elevated temperatures as the system cools down from a cubic austenitic state.

In addition to the structural search results, we also present total energy calculations for the Burgers transformation and Bain paths in the conventional Heusler and inverse Heusler Co_2NiGa alloys. It is postulated that the isolation of a low-energy martensitic phase which is more stable than the $L1_0$ martensite via *ab initio* calculations may be attributed to a classic case of the phase selection conundrum, wherein the Co_2NiGa $L2_1$ phase preferentially transforms to the $L1_0$ martensitic phase in spite of other possible structures which are inaccessible even though their energy is lower. Elastic and phonon calculations were carried out with the intention of isolating any instabilities due to vibrational or elastic effects . Finally, the Bain and Burgers paths were recalculated taking into consideration the effect of configurational , magnetic, and atomic disorder. This analysis indicates that there is probably a good explanation of why we do not observe the other phases predicted from the structural search.

The organization of this paper is as follows: In Sec. 4.1 the computational details and methodology used to perform the calculations is outlined. In Sec. 4.2 the Bain and Burgers transformations are applied to austenitic Co_2NiGa and the results are presented. Sec. 4.3 outlines the minima hopping method as used in this work and the results obtained therein. The phase selection hypothesis is presented and calculations carried out to validate it are discussed in Sec. 4.4. Finally conclusions are drawn in Sec. 4.6 and the work done is summarized.

4.1 Computational Details and Methodology

The results presented in this work are *ab initio* calculations carried out to determine the electronic, structural, and elastic properties of Co_2NiGa stoichiometric Heusler alloys. The calculations were performed within the framework of density functional theory, as implemented in the Vienna *ab initio* simulation package (VASP)[23], applying the generalized gradient approximation (GGA) using the Perdew-Wang 1991 (PW91) functional [55]. Single - parameter Burgers path calculations were also carried out using the local density approximation (LDA) [76]. The electronic configurations of the relevant elements were realized using the projector augmented wave (PAW) pseudo-potentials formalism [26]. Brillouin zone integrations were performed using a Monkhorst-Pack mesh [56] with at least 5000 k points per Brillouin zone or cell. Full relaxations were realized by using the Methfessel-Paxton smearing method of order 1 [57], and self-consistent static calculations were carried out with the tetrahedron smearing method with Blöchl corrections [58]. A cutoff energy of 350 eV was used for all the Bain and Burgers path calculations and spin polarizations were accounted for as well. Convergence of the electronic structure was assumed, when changes between two consecutive steps fell below $10^{-7} eV$.

The elastic constants were calculated by imposing a set of strains on the crystal structure $\epsilon = (\epsilon_1, \epsilon_2, \epsilon_3, \epsilon_4, \epsilon_5, \epsilon_6)$ [32, 33, 34, 35, 36]. The stresses (σ_i) resulting from the change in energy due to the deformation are calculated. By application of Hooke's law $\sigma_i = C_{ij}\epsilon_j$, the stiffness tensor C_{ij} may be computed. The bulk modulus (B) is calculated by[36]:

$$B = \frac{2}{9}\left(C_{11} + C_{12} + 2C_{13} + \frac{C_{33}}{2}\right) \qquad (4.1)$$

The shear modulus is calculated using the Voigt approximation [36],

$$G = \frac{1}{15}\left(2C_{11} + C_{33} - C_{12} - 2C_{13}+\right) + \frac{1}{5}\left(2C_{44} + \frac{1}{2}(C_{11} - C_{12})\right) \qquad (4.2)$$

while Young's modulus is computed by [36]

$$E = \frac{9BG}{3B + G} \qquad (4.3)$$

and Poisson's ratio may be calculated as :

$$\nu = \frac{E}{2G} - 1 \qquad (4.4)$$

4.2 Transformation paths in Co_2NiGa

The crystallographic relations for the b.c.c-h.c.p transformation were established by Burgers [72] and can be described as:

$$(110)_{b.c.c} \parallel (0001)_{(h.c.p)} , \qquad [\bar{1}11]_{b.c.c} \parallel [\bar{2}110]_{h.c.p} \qquad (4.5)$$

The transformation manifests in the form of two collective movements of atomic planes: (i) shearing towards the $[\bar{1}11]$ direction along the $(1\bar{1}2)$ plane transforming the (110) b.c.c plane into the (0001) h.c.p plane, and (ii) shuffling of alternate (110) planes in the $[0\bar{1}10]$ direction ,with a constant (110) interplanar distance. The Burgers mechanism thus involves two distinct and simultaneous structural changes characterized by primary order parameters.
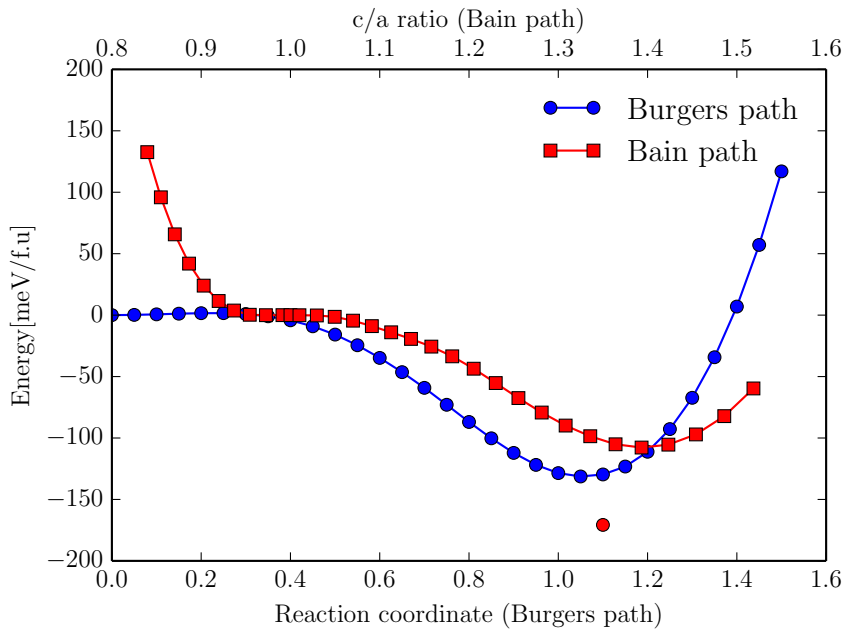
Figure 4.1: Energy profile comparison for Bain and Burger paths in Co_2NiGa . The minimum along the Burgers path occurs at approximately $\delta = 1.1$ (O structure). The single data point in the figure corresponds to the completely relaxed minimum energy structure.

4.2.1 1-parameter Burgers path

Friak et al. [77] coupled the two degrees of freedom to obtain a single-parameter Burgers path to study the b.c.c-h.c.p transformation in iron [78, 79, 77]. This model is modified and applied to the $L2_1 \rightarrow hcp$ transformation in this work. Proceeding in a manner similar to [77], the simplest transformation is accomplished using an orthorhombic basis applied to a 1x2x1 supercell of a 4-atom unit cell. For a $L2_1$ lattice constant a , the orthorhombic lattice parameters will be

$$a_0 = \frac{\sqrt{2}a}{s(\delta)^{1/3}}; \qquad b_0 = a\left(\frac{\delta(2\sqrt{3} - 3\sqrt{2})}{6} + \frac{\sqrt{2}}{2}\right); \qquad c_0 = a\left(\frac{\delta(2\sqrt{2} - 3)}{3} + 1\right)$$

$$(4.6)$$

34

where:

$$s(\delta) = \sqrt{2}\ \left(\frac{\delta(2\sqrt{3} - 3\sqrt{2})}{6} + \frac{\sqrt{2}}{2}\right) \cdot \left(\frac{\delta(2\sqrt{2} - 3)}{3} + 1\right) \tag{4.7}$$

Here, $\delta = 0$ corresponds to the $L2_1$ phase and $\delta = 1$represents the hcp phase. Correspondingly, the angle in the (110) $L2_1$ planes evolves from $\theta = 109.47°$ to $\theta = 120°$. The (110) $L2_1$ planes are transformed to the (0001) hcp stacking planes.

In Figure 4.1, we present the profile of the differential energy (δE) along the Bain path and single-parameter Burgers paths for $CoNiGa$. For the Burgers path, $\delta = 1$ corresponds to the perfect hcp lattice type. It is seen that the minimum along the Burgers path occurs at approximately $\delta = 1.1$. The single data point in the figure corresponds to the completely relaxed minimum energy structure. The energy of this structure is noted to be further lowered by about 50 meV upon complete relaxation.

4.2.2   2-parameter Burgers path

When both degrees of freedom are considered, this gives rise to the Burgers surface which determines the energy field for the transformation. Nishitani et al [80] described the b.c.c-h.c.p transformation in Ti using the Burgers surface by performing first-principle calculations using a two-parameter model corresponding to the above mentioned two degrees of freedom.

In order to model the Burgers surface of the Co_2NiGa and Co_2NiAl Heusler alloys, keeping the atomic volume constant, the most rigorous transformation path is achieved by using an orthorhombic basis (space group :CmCm, #59, Pearson symbol:$oS4$) in conjunction with an 8-atom unit cell. The evolution of the basis vectors and atom positions gives rise to a two-dimensional parameter space (δ, η), where δ_1 accounts for the basal shear and η for the shuffle. For a $L2_1$ lattice constant

a, the orthorhombic lattice parameters will be

$$a_0 = a\sqrt{2} \; ; \tag{4.8a}$$

$$b_0 = 2a/s(\delta) \; ; \tag{4.8b}$$

$$c_0 = a\sqrt{2}s(\delta) \tag{4.8c}$$

where:

$$s(\delta) = 1 + \left[\left(\frac{3}{2}\right)^{0.25} - 1\right]\delta \tag{4.9}$$

The basis vectors are given by $[a_0, 0, 0], [0, b_0, 0], [0, 0, c_0]$. The atomic positions are specified as $(0, 0.25, 0.5)$, $(0, 0.75, 0)$, $(0.5, 0.25, \eta/6)$, $(0.5, 0.75, \eta/6)$, $(0, 0, 0)$, $(0.5, 0.5, 0.5 + \eta/6)$, $(0, 0.5, 0)$ and $(0.5, 0, 0.5 + \eta/6)$. The L_21 and hcp phases then correspond to (0,0) and (1,1) respectively.

Figure 4.2, shows the Burgers energy surface for the Co_2NiGa Heusler alloy considering a two-parameter Burgers path that takes explicit account for shuffles and shears necessary to transform a bcc lattice into an hcp variant. In the figure, $(0, 0)$ corresponds to the $L2_1$ structure and $(1,1)$ corresponds to an hcp-like structure.

For these calculations, a 17x17 grid was used and the energy of the intermediate structures at each grid point was calculated using methods detailed in Sec. 4.1. A second-order accurate finite difference scheme was then used to compute the total energy surface. The minimum energy path (MEP) for the Burgers transformation through this energy surface was constructed by using the modified string method [51]. This method allows determination of the MEP by finding the minimum energy configuration along the hyperplanes normal to the path. The MEP for the Burgers transformation is also indicated along the surface. The inset shows the energy pro-
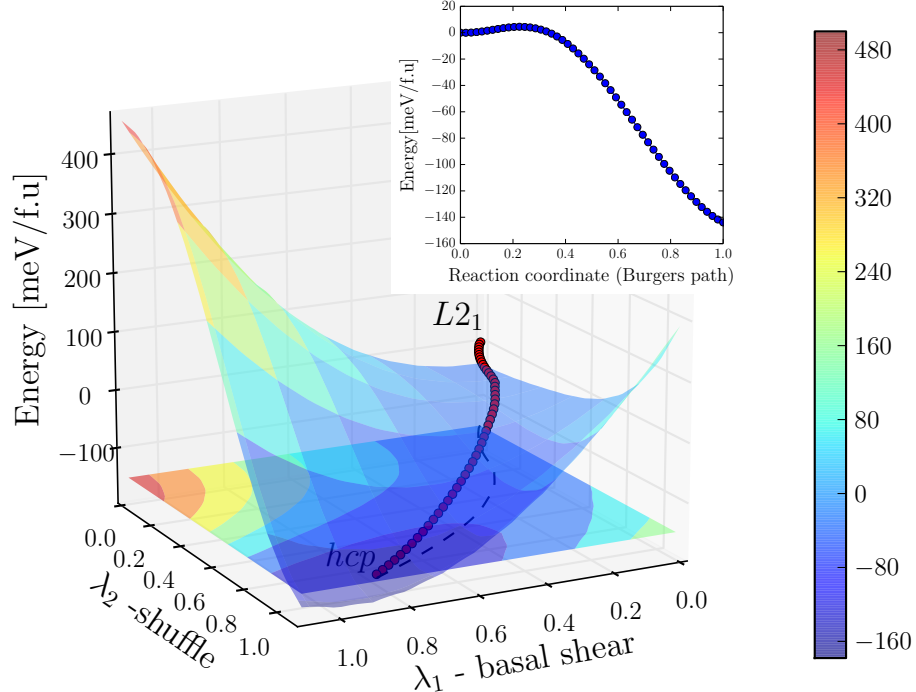
Figure 4.2: Burgers energy surface for Co_2NiGa Heusler alloy. $(0,0)$ corresponds to the $L2_1$ structure and $(1,1)$ corresponds to the hcp structure. Inset: Energy profile for the transformation.

file of the transformation, which is again barrierless. The energy values for all the different fully relaxed structures along with their lattice parameters are summarized in Table 4.1.

From Table 4.1, it is seen that both the 1-parameter and 2-parameter Burgers paths yield a stable orthorhombic phase appreciably lower in energy than $L1_0$ via barrier-less transformations. Subsequently, it was deemed necessary to explore the energy landscape surrounding the $L1_0$ structure by applying the minima hopping methods, results of which are detailed in the following section.

4.3   Minima Hopping Method

Minima hopping calculations were carried out for the Co_2-Ni-Ga chemical composition. The basics of the method are described in detail in the original references

Table 4.1: Lattice parameters and ground state energies. Calculations were performed using the GGA [55] approximation. Energy difference is computed relative to the $L1_0$ structure in $meV/f.u$

Model	Structure	Space Group	a (Å)	b (Å)	c (Å)	δE (meV/f.u)
	$L2_1$	225	4.015	4.015	4.015	108.402
	$L1_0$	123	4.364	4.364	3.598	0.000
1-param	O	59	4.113	5.094	4.397	-68.747
2-param			4.484	5.084	4.073	-118.436

[40, 81]. In summary, this method performs a systematic *ab initio* search for low-enthalpy phases of a given compound, where the only input is the chemical composition and the number of atoms in the simulated cell. Short Rahman-Parrinello molecular dynamics simulations [82], are used to escape from local minima and efficient local geometry relaxations were performed to identify stable configurations. The efficiency of the escape step was ensured by aligning the initial atomic velocities within the molecular dynamics along a soft mode direction. The energy and stresses are obtained by interfacing the method with VASP [23]. As in the total energy calculations, the projector augmented wave (PAW) method was used to describe valence and core electrons [26]. To approximate the exchange-correlation functional we used the Perdew-Burke-Ernzerhof (PBE) [83] generalized gradient approximation. After the potential structures are found by the minima hopping method, the structure is tightly minimized by using a plane wave cutoff of 550 eV, and the k mesh used to calculate the observables in the Brillouin zone is adapted such that the calculation guaranteed a numerical convergence of the total energy to less than 2 meV/atom. The structures were also re-optimized by using other functionals in accordance with the total energy calculations.

A summary of the results is shown in Table 4.2. This table shows the energy of

Table 4.2: Energy difference of the predicted crystal structures in $meV/f.u$ for Co_2NiGa

Space Group	δE GGA	PBE	LDA	Structure
123	0	0	0	$L1_0$
3	-58.0920	-21.2160	-67.1520	monoclinic
5	-55.5360	-51.1120	-82.5480	monoclinic
8	-109.976	-100.936	-150.396	monoclinic
11	-139.124	-136.228	-167.192	monoclinic
12	-122.636	-115.444	-159.772	monoclinic
31	-104.456	-99.6720	-136.620	orthorhombic
40	-66.2120	-61.1280	-91.3280	orthorhombic
44	-78.9040	-71.2440	-117.124	orthorhombic
51	-68.9520	-75.6160	-61.2120	orthorhombic
59	-132.536	-144.816	-151.376	O
63	-125.012	-126.512	-152.972	orthorhombic
119	-137.296	-131.360	-183.000	tetragonal
139	-27.9680	-20.7720	-67.9200	tetragonal
216	83.3960	89.4600	94.6720	Inv. Heusler
225	108.402	109.232	78.2080	$L2_1$

all structures using GGA [55], PBE [83], and LDA [76] approximations relative to the relaxed $L1_0$ structure. It is seen that a number of structures with monoclinic, tetragonal and orthorhombic symmetries are predicted with energies much lower than the $L1_0$ structure. The list also includes the O phase, which was observed in section 4.2 to result from a Burgers transformation of the original $L2_1$ structure. This shows that a number of low-energy structures theoretically exist in the thermodynamic vicinity of $L1_0$ but have been inaccessible experimentally.

Figure 4.3 shows the simulated x-ray diffraction spectra for some of the lowest-energy structures, that can be used by the experimentalist to compare with some of our-low energy structures. The transformation mechanisms for all these structures, except the O structure, are unknown. The possibility of considering all possible
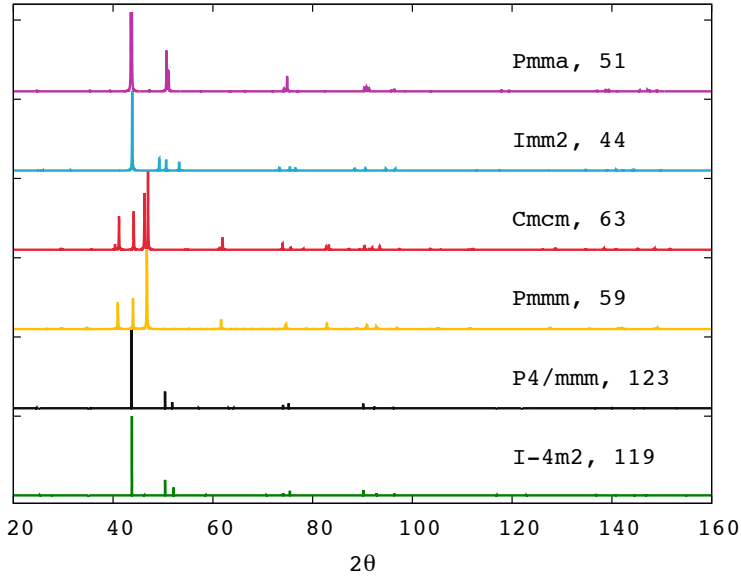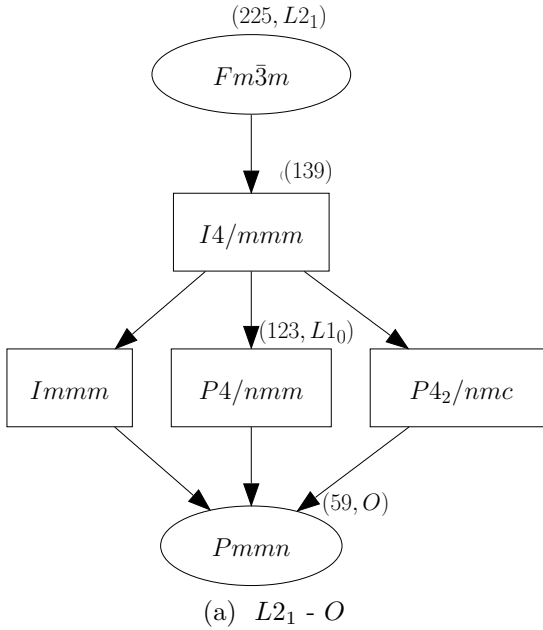
Figure 4.3: X-ray diffraction spectrum with Cu Kα radiation, λ=1.54178 Å for some of the low-energy structures reported in Table 4.2x.

structural transitions from the $L1_0$ phase to the predicted ones is not the focus of this paper. Instead, we focus only on the O structure and conduct a thorough analysis to investigate (i) the stability of the structure and (ii) the possible energy barriers which may render these low-energy structures inaccessible.

4.4 Analysis and Discussion

As mentioned earlier, the austenitic phase in the Heusler system Co$_2$NiGa has a $L2_1$ structure. The martensitic transformation exhibited by this alloy is reversible, giving rise to the shape memory effect. This implies that the resultant martensite has a symmetry which is a sub-group of the austenitic cubic structure [87]. The point group symmetries of the relevant structures are $Fm\bar{3}m$. for $L2_1$, $P4/mmm$ for $L1_0$, and $Pmmn$ for the O phase. The point groups of both the $L1_0$ and the O structures are sub-groups of the $L2_1$ point group. The group - subgroup relationship for the (a) $L2_1$-O and (b) $L2_1$-$L1_0$ are shown in Figs. 4.4a and 4.4b. Three possible

40
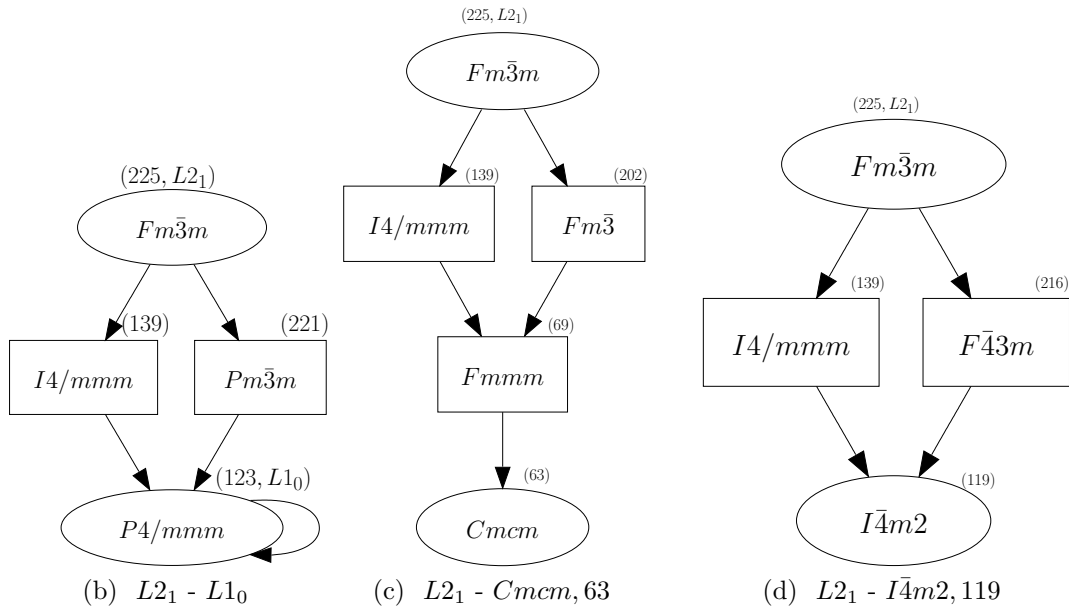
Figure 4.4: Group-subgroup graphs for (a) $L2_1$-O,(b) $L2_1$-$L1_0$,(c) $L2_1 - 63$, and (d) $L2_1 - 119$.These were generated using the Bilbao crystallographic server [84, 85, 86]. Space groups corresponding to the relevant point groups are indicated.

paths exist for the symmetry transformation from $L2_1$ to O while two paths exist for the symmetry transformation from $L2_1$ to $L1_0$. Some examples of group-subgroup

relations for additional structures isolated using the minima hopping method, which are close in energy to the O structure, viz., structures corresponding to space groups #63 and #119, have been described in Figs. 4.4c and 4.4d. For both of these structures, we have two possible symmetry-reducing transformations. Of all the structures listed in Table 4.2, structures with space groups 12, 51, 59, 63, 119, 123 and 139 satisfy the symmetry relations with number of symmetry paths ranging between 1 and 5. For space groups 8 and 11, symmetry relations are satisfied, but the number of symmetry paths is 15 and 12, respectively. A larger number of possible symmetry paths amounts to a one to many correspondence, which makes it harder for a material to "remember" it's original crystal structure, thereby hindering the ideal shape memory effect. The remaining structures (space groups 3, 5, 31, 40, 44) do not satisfy the symmetry requirements. Thus, from a crystallographic point of view, it is seen that in addition to the O phase,a number of other structures also satisfy requirements.

The ideal reversible martensitic transformation must also be a volume-preserving transition [87] since the higher the volume change, the greater is the hysteresis or irreversibility associated with the transformation. Having established the fact that there is a group-subgroup relation between $L2_1$ and the O phase, we proceeded to investigate the existence of possible barriers to the transformation. Table 4.3 shows the volume change (δV) associated with the $L2_1$-O and $L2_1$-$L1_0$ transformations , the effective bulk modulus for the transformation (B_e) , the corresponding volumetric strain energy per unit volume (E_v), and the total energy for the transformation (E_t). The volumetric strain energy was calculated as

$$E_v = \frac{1}{2}\sigma_v \epsilon_v = \frac{1}{2}(B_e \epsilon_v)\epsilon_v = \frac{1}{2}B_e {\epsilon_v}^2 \tag{4.10}$$

Table 4.3: Energy difference due to volume changes during transformation. Indicated are the volume change (δV) for the transformations , the effective bulk modulus for the transformation (B_e) , the corresponding volumetric strain energy per unit volume (E_v) and the total energy for the transformation (E_t).

Transformation	δV ($\mathring{A}^3$)	B_e (GPa)	E_v ($meV/f.u$)	E_t ($meV/f.u$)
$L2_1$ - O	-0.28	145	-0.784	-226.838
$L2_1$ - $L1_0$	-0.12	142.5	-0.141	-108.402

where σ_v is the volumetric stress and ϵ_v is the volumetric strain. ϵ_v was calculated by taking the ratio of change in volume (δV) to original volume. B_e was estimated by averaging the bulk moduli for the austenitic and martensitic phases. In Table 4.3, it is apparent that the volumetric strain energy associated with the $L2_1$ - O is about 5 times larger than that for the $L2_1$ - $L1_0$ transformation; however when compared to the E_t, it it seen that its contribution is negligible. Also, one must keep in mind that bulk effects (such as those associated with elastic strain energy) only become important as the system volume becomes large enough. The possible nucleation of the O phase from a parent $L2_1$ matrix is thus not ruled out.

4.4.1   The phase selection problem

Recapitulating, the Co_2NiGa Heusler alloy shows a phase transformation from the austenitic, high-temperature $L2_1$ structure to the martensitic, low-temperature non-modulated $L1_0$ phase. Minima hopping calculations predict a number of structures with monoclinic, tetragonal and orthorhombic symmetries with energies much lower than the $L1_0$ structure. Furthermore, Burgers path calculations predict the existence of a martensitic phase with orthorhombic symmetry , the O phase. This phase is stable against perturbations along a Burgers transformation in a barrier-less
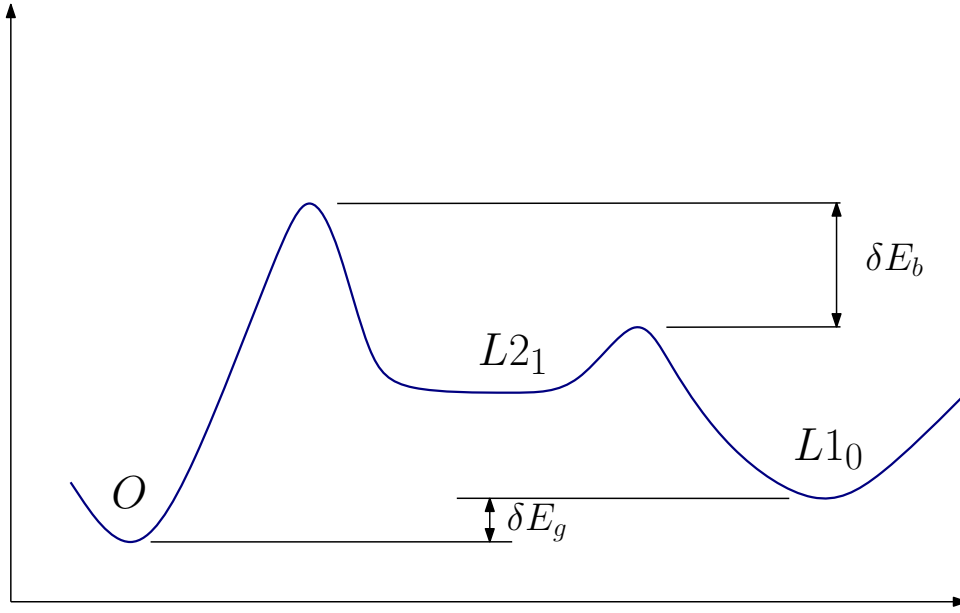
Figure 4.5: Schematic of relative stabilities of the $L1_0$ and the O structures. δE_g is the energy difference between the conventional martensitic phase $L1_0$ and the O phase. δE_b is the proposed difference between the energy barriers for the $L2_1$- O transformation and the $L2_1$ - $L1_0$ transformation.

fashion. While the examination of possible elastic energy barriers to the transformation suggested that there maybe some elastic constraints to the stabilization of the O phase, the elastic energy may not be sufficient to completely rule it out.

It is proposed that the absence of the O phase may be attributed to the problem of phase selection. As seen in Figure 4.5 , a possibility exists that while the O phase is relatively more stable than the $L1_0$ phase , the energy barrier for the $L2_1$ -O transformation may be higher than the barrier to the $L2_1$ -$L1_0$ transformation, i.e, $\delta E_b > \delta E_g$ at some temperature far away from the ground state conditions, when the system is cooled from the $L2_1$ structure. In this case, the high temperature austenitic phase may not be able to sample a subset of low energy states since there may be no accessible paths. We proceeded to examine the stability of the O phase in terms of its vibrational spectrum, its elastic constant tensor and we also examined the effect of

44

configurational and magnetic disorder (brought about by high temperatures) on the competition between Bain and Burgers paths, taking the $L2_1$ structure into either the observed $L1_0$ or the missing O phase. .

4.4.2   Vibrational properties

Phonon calculations were carried out to study the relative stability of the $L2_1$, $L1_0$, and O structures. We used the FITFC module as implemented in the ATAT package to perform the vibrational calculations. In this method [27, 28], the positions of the atoms are slightly perturbed away from their equilibrium position and the reaction forces are calculated. A set of linear constraints are obtained by equating the calculated forces to the forces predicted from the harmonic model. From these, the unknown force constants are determined. The force constant matrix is then used to extract the projected vibrational density of states and the phonon dispersion curves. The projected vibrational density of states is shown in Figure 4.6 .

The mode of interest in these alloys is along the [110] direction. The calculated phonon dispersion curves of the three structures were compared. Figure 4.7 shows the projected vibrational density of states for these structures along the $[\xi, \xi, 0]$ directions in the Co_2NiGa systems. No unstable modes are observed. Softening of the optical modes is observed in the $L1_0$ as well as the O structures. No conclusions can be drawn about the relative stability of the structures. The vibrational contribution to the total energy was estimated for the three structures by integrating over the vibrational density of states. However, the contributions were negligible (< 5meV); hence we do not include them in this work.

4.4.3   Elastic properties

Elastic constants for the structures considered in this work were calculated as explained in Sec. 4.1 and are listed in Table 4.4 in GPa. Included are the significant

45
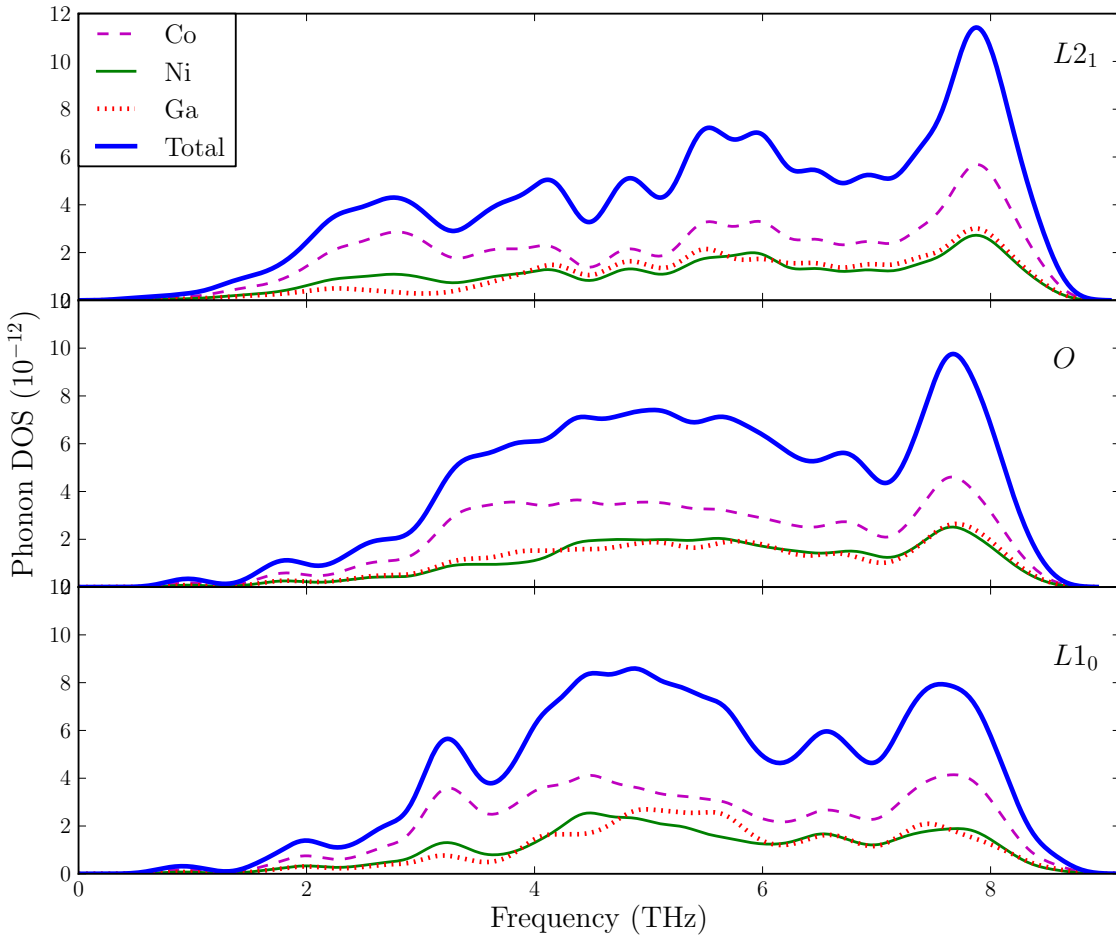
Figure 4.6: Projected vibrational density of states for the Co_2NiGa system at $T = 0$ K.

components of the stiffness tensor (c_{11} , c_{12} , c_{13} , c_{33} and c_{44}) , bulk modulus (B), shear modulus (G), elastic modulus (E), and Poisson's ratio (ν). From the table we see that the elastic moduli of $L1_0$ and O structures are close in magnitude. There is no suggestion of instability. $C_{11} - C_{12}$ lends an insight into the stability of the structure with respect to shear and other martensitic transformation inducing deformations. For the $L2_1$ structure, $C_{11} - C_{12} < 0$, which is expected since the $L2_1$ structure is unstable with respect to temperature and undergoes a martensitic transformation.

46
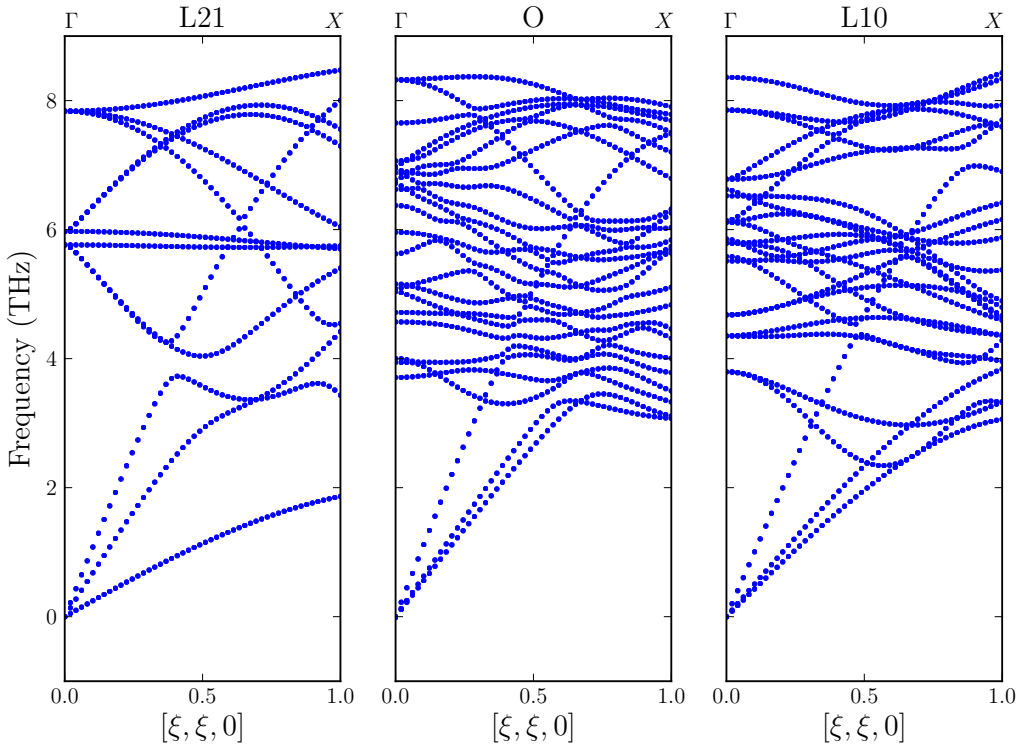
Figure 4.7: Phonon dispersion curves along the $[\xi, \xi, 0]$ direction for the Co_2NiGa system at $T = 0$ K.

However $C_{11} - C_{12}$ values for both $L1_0$ and O structures are positive, with the value for the O phase being higher indicating increased stability with respect to the $L1_0$ structure.

4.5 Effect of disorder on the competition between Bain and Burgers paths

While arguments using rough estimates for the elastic strain energy associated with the $L2_1 - L1_0$ and $L2_1 - O$ transformations suggest a higher elastic barrier for the latter, these arguments cannot be used when looking at the incipient process of the formation of a new phase out of the $L2_1$ matrix since at early stages of the phase transformation bulk energy contributions may not be significant enough. On the other hand, the phonon and elastic calculations suggest that the O phase is

Table 4.4: Calculated elastic properties of $CoNiGa$ in GPa. Significant components of the stiffness tensor (C_{ij}), bulk modulus (B), shear modulus (G), elastic modulus (E) and Poisson's ratio (ν) are indicated. Calculations were performed using the GGA [55] approximation.

Alloy	Structure	c_{11}	c_{12}	c_{13}	c_{33}	c_{44}	B	G	E	ν
$CoNiGa$	$L2_1$	181	186	186	181	141	136	52	139	0.33
	$L1_0$	252	153	163	204	114	149	71	184	0.29
	O	265	154	108	328	55	154	66	173	0.31

mechanically stable. This leads us to believe that there exist mechanisms arising from hitherto unaccounted for contributions within the material which make these low energy states inaccessible when coming from high-temperature experiments. We thus proceed to examine three such contributions: (i) the effect of configurational disorder, (ii) magnetic disorder, and (iii) atomic disorder.

4.5.1 Effect of configurational disorder

It is well known that atomic ordering may influence the transformation behavior of SMAs. Substantial experimental and numerical work has been carried out in investigating the order-disorder transition, long-range ordering, and effect of ordering on the phase transformation characteristics in various shape memory alloys [88, 89, 90]. Recarte *et al.* show that in Ni-Mn-In SMA, the thermodynamics of the martensitic transformation depends on the atomic ordering [90]. The effect of configurational disorder was simulated by using special quasirandom structures (SQS) [91], implemented using the ATAT toolkit. A 32-atom supercell was used and the Bain and Burgers paths were recalculated for this structure and are shown in Figure 4.8. We see that the energy at the minimum along the Bain path is still higher than that along the Burgers path, although the energy difference is substantially lowered
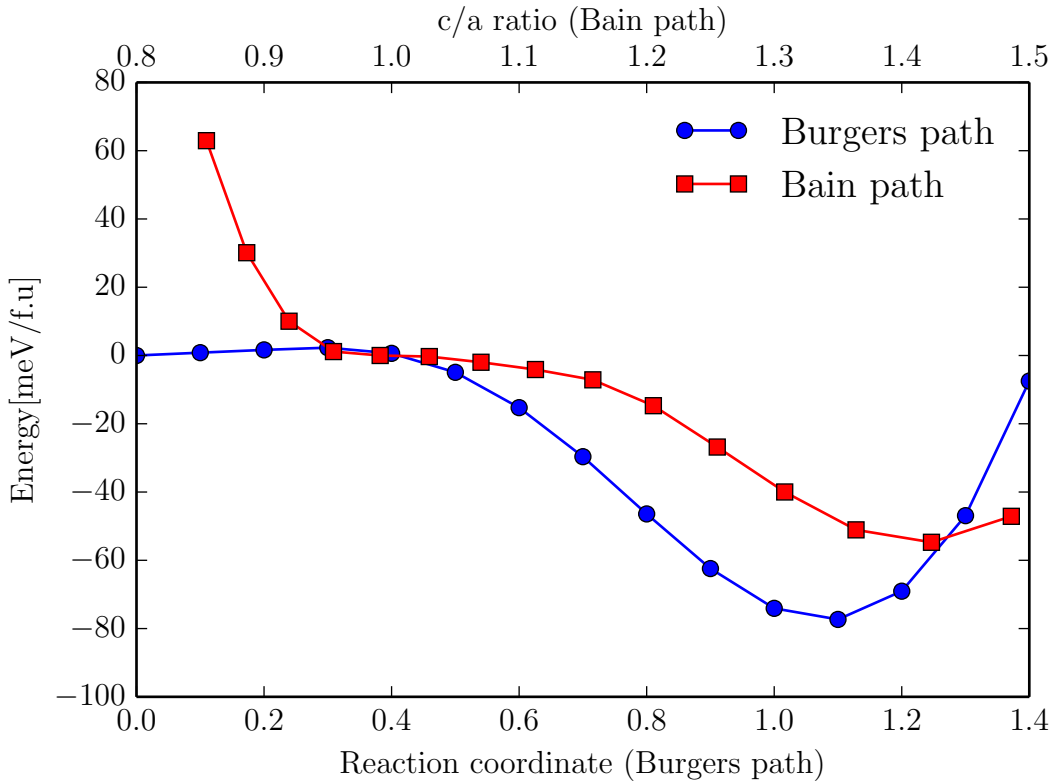
Figure 4.8: Energy profile comparison for Bain and single parameter Burger paths in disordered (SQS) Co_2NiGa

$(\approx 25meV)$.

4.5.2 Effect of magnetic disorder

In this sub-section, we present Bain path and Burgers path calculations for varying degrees of magnetization ($100\% - 0\%$). This may be viewed as a crude method to simulate the effect of high temperatures by lowering the magnetization. This is achieved by using the fixed spin moments method within VASP. Specifically, we assign a value to the parameter NUPDOWN in the INCAR file. Fixing the value of this parameter ensures that the difference of the number of electrons in the up and down spin component will be kept fixed to the specified value. We calculate the

Bain and Burgers paths for the different values of NUPDOWN. For these calculations, VASP automatically sets MAGMOM = NUPDOWN/number of ions; hence we use the term MAGMOM to denote the different cases. Results are presented for 100 %, 90 %, 70 %, 50 %, 30 % magnetic moment values and the non-magnetic case.

In Figure 4.9, it is seen that for the 100 % MAGMOM case, as seen before, the Burgers path has a lower minima than the Bain path; i.e., the O phase is more stable than the $L1_0$ phase. However, on lowering the magnetic moment, as in Figure 4.9 (b), the Burgers and Bain paths have almost coinciding minima. On further lowering the magnetic moment as in Figure 4.9(c) - 4.9(f), the trend is reversed and the Bain path is seen to have an increasingly lower minima than the Burgers path. Thus reducing the magnetization of the system, i.e., introducing magnetic disorder and simulating the effect of higher temperatures, stabilizes the $L1_0$ phase with respect to the O phase.

4.5.3 Effect of non-stoichiometric composition

In this section we account for the effect of atomic disorder, viz, the modeling of the transformation in a non-stoichiometric composition. As observed in [60], it is not simple to achieve the perfect Heusler composition Co_2NiGa because one is very near the two-phase $(\gamma + \beta)$ region or at the border of the $B2$ phase. Simulating a non - stoichiometric composition also weakens the magnetic ordering naturally (as opposed to fixed-spin calculations in Sec. 4.5.2). We use a 16-atom SQS supercell to model the the $Co_{43.75}Ni_{25}Ga_{31.25}$ composition and calculate the Bain path. Since the symmetry of the structure is lowered due to the off - stoichiometric composition, the Bain path (varying of c/a) was calculated for 2 cases: (i) $c||z$ and (ii) $c||y$. We then selected the Bain path with the lower energy profile. For the Burgers path, we used a simple 16-atom supercell to simulate the structure. Since Ga replaces Co,

(a) A (b) B

(c) C (d) D

(e) E (f) F
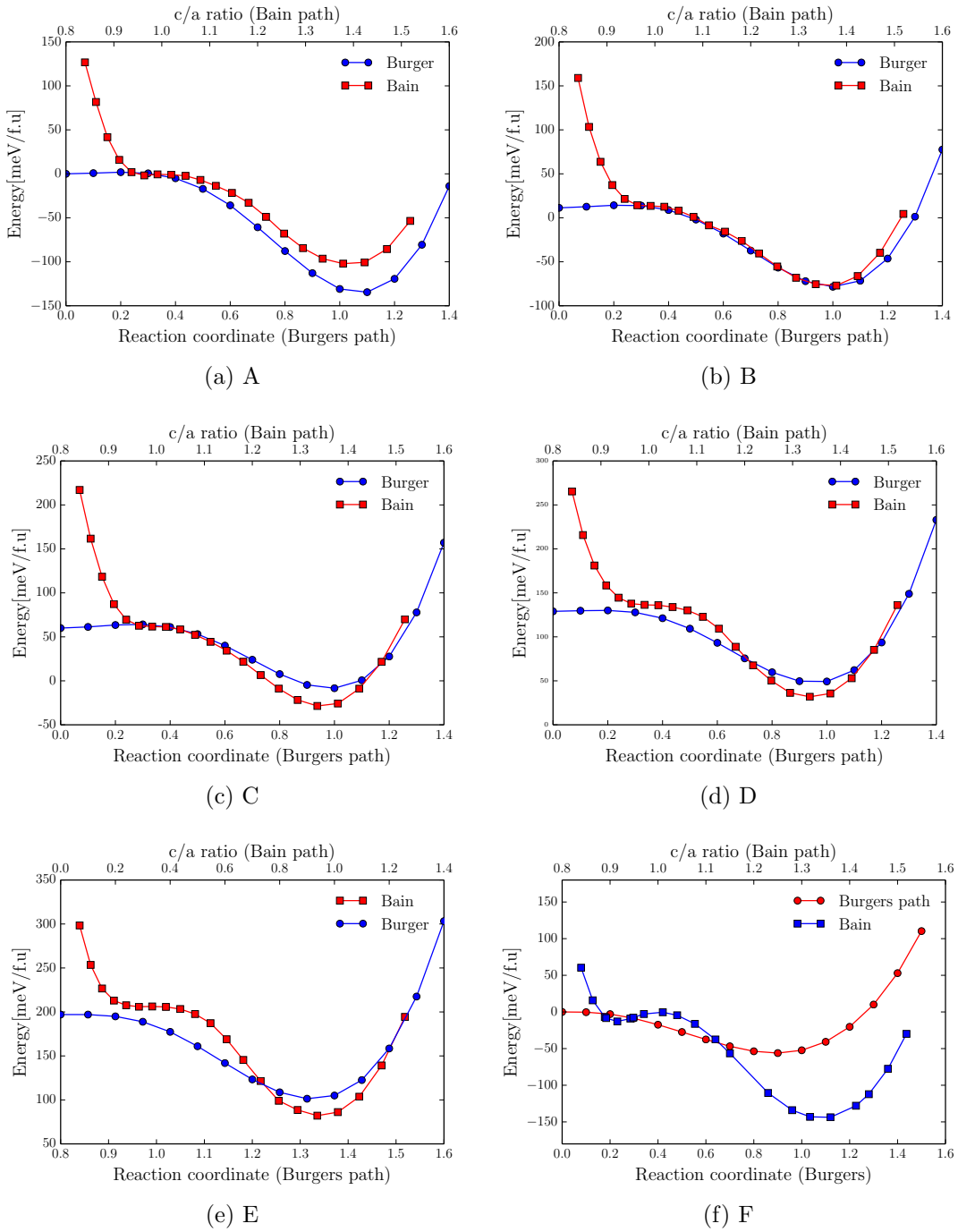
Figure 4.9: Energy profile comparison for Bain and single parameter Burger paths in Co_2NiGa for varying values of magnetization (fixed spin moment calculations)
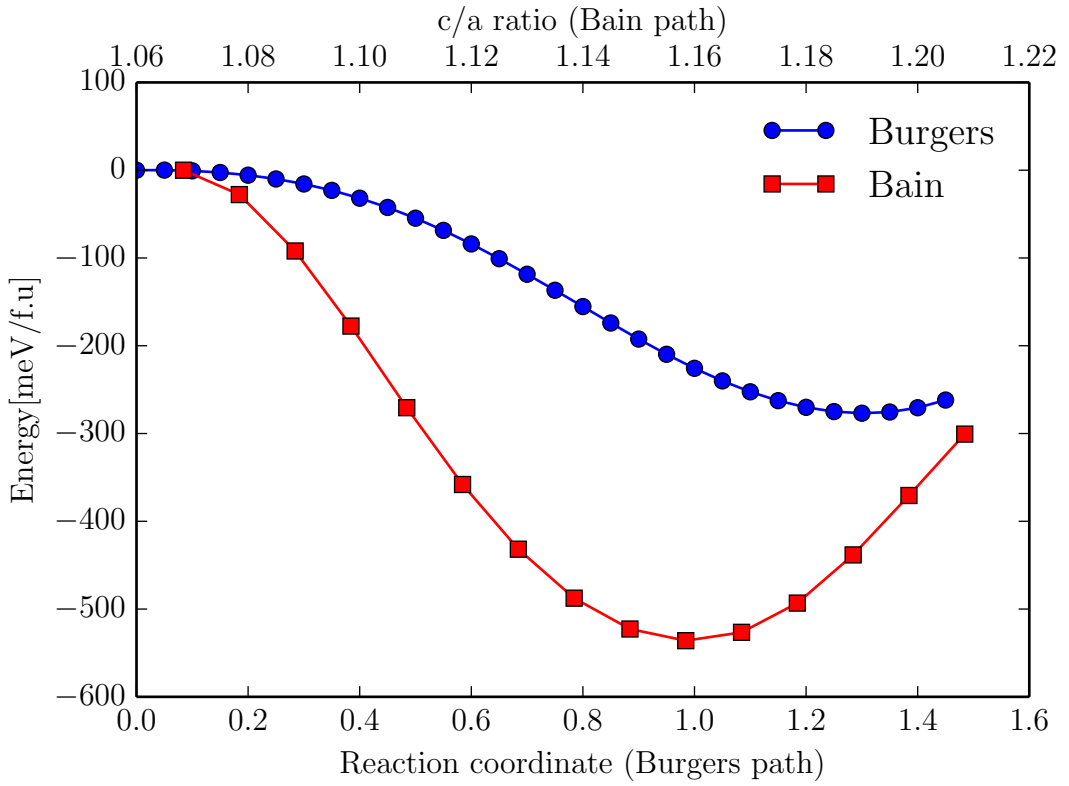
Figure 4.10: Energy profile comparison for Bain and single parameter Burger paths in $Co_7Ni_4Ga_5$.

we considered all possible configurations of Ga replacing Co and then selected the lowest energy configuration. The Burgers path was carried out on the lowest energy configuration. Thus it was ensured that the lowest possible Bain path and Burgers paths were used, which encapsulate all possible energy ranges which may be observed and enable us to make a qualitative, if not quantitative observation. The results are indicated in Figure 4.10. It is seen that the $L1_0$ structure as achieved through the Bain path is more stable than the corresponding O phase for this composition. This may be attributed to the weakening of the magnetic ordering due to substitution of one Co atom by a Ga atom, as mentioned earlier .

4.6   Summary and Conclusion

The Burgers path was investigated in the Co-Ni-Ga ferromagnetic shape memory alloy system. Calculations were carried out using two models: a single-parameter characterization of the Burgers path and a two-parameter Burgers model which generates a transformation energy surface. In both models, a low-energy structure with an orthorhombic symmetry (O) is observed whose parameters are shifted from the expected co-ordinates for the transformation. This low energy structure (O) has been unobserved experimentally. Complete relaxation of the O structure shows further reduction in energy. The Bain path for the alloys is also determined and compared to the Burgers path. Minima hopping calculations were carried out to investigate the energy landscapes surrounding the $L1_0$ martensitic phase in $Co - Ni - Ga$. Results showed the existence of a number of structures similar in energy to as well as much lower than the predicted O phase in the vicinity of the $L1_0$ structure. It was postulated the the Co_2NiGa Heusler system exhibits a classic case of the phase selection problem. Although the unexpected Ophase may be relatively more stable than the $L1_0$ phase, the energy barrier for the $L2_1$ -O transformation may be much higher than the barrier to the $L2_1$ -$L1_0$ transformation. This high barrier may be due to vibrational effects, elastic effects, configurational disorder, magnetic disorder, or due to micro-structural effects.

In an effort to validate this hypothesis, the stability of this structure was investigated via elastic and lattice dynamics calculations and the contributions of configurational and magnetic disorder on the transformations were studied. No instabilities due to vibrational effects were detected. Elastic calculations showed comparable values of elastic properties for the $L1_0$ and O phases. $C_{11} - C_{12}$ values showed that the O phase is relatively more stable than the $L1_0$ phase. Calculations incorporating

configurational disorder showed a lowering in the energy difference between the $L1_0$ and the O structures, but the O structure was still more stable. The calculations simulating the effect of magnetic disorder/ high temperature showed that the $L1_0$ structure may be stabilized with respect to the O phase by lowering the magnetic moment. Thus, it is proposed that magnetic disorder plays an important role in the phase selection energetics of the $CoNiGa$ system and is a principal contributor in the determination of the transformation path followed in this system. Further calculations were carried out on an off-stoichiometric composition $Co_{43.75}Ni_{25}Ga_{31.25}$, where the weakening of the magnetic ordering manifests naturally. As expected, the $L1_0$ phase was seen to be more stable than the O phase.

Reverting to the question raised earlier, we conclude that it is unrealistic to use standard DFT prototypes to investigate ground states of relatively less known systems. By performing a detailed analysis of the transformation paths (Burgers and Bain) by taking into account perturbations on the ground state, it is seen that what is manifested is in principle a phase selection problem: the ultimate crystal structure that the system transforms into, depends on the path that the system prefers. When coming from high temperature, the accessible path is that corresponding to the Bain transformation. To conclude, discrepancies between DFT and experiments may be reconciled if we consider the 'history' of the alloy.

5.   PARAMETRIC MODELING OF THE $B2 - B19'$ TRANSFORMATION IN $NI - TI$ SMA

5.1   Introduction

$Ni - Ti$ is the most well-known practical SMA available today. It has excellent mechanical properties and exhibits the shape memory effect which contribute to make it a very viable material for multi-functional applications. Current practical uses are however, limited to temperatures below 100 °which is the transformation temperature limit of near equiatomic $Ni - Ti$ binary alloy [59]. $Ni - Ti$ SMA, or Nitinol, as it is commercially known, was first discovered by Buehler in 1963 [6]. Today, commercially it is used extensively in the medical engineering world. The human body offers an isothermal environment which takes away many of the design complexities and disadvantages of Nitinol.

The $Ni - Ti$ system is fundamentally very complex and exhibits interesting competing martensitic transformations. Depending on the composition and the heat-treatment it is subjected to, it has various important phases. The high-temperature symmetric austentic phase is B_2 (CsCl, space group $Pm\bar{3}m$ 221). On cooling under certain specific conditions, $Ni - Ti$ may undergo a initial martensitic transformation characterized by a sharp increase in resistivity and low hysteresis [92]. This initial martensitic transformation is referred to as the R-phase transformation and results in a trigonal phase. On further cooling, the R phase undergoes a second martensitic transformation with a large hysteresis results in the low-temperature martensitic phase - the monoclinic B19' (space group $mP4$, 11). Another phase of import is the intermediate orthorhombic phase $B19$ (AuCd, space group $Pmma$, 51). It is widely postulated to be an intermediate phase in the $B2 - B19'$ transformation, although it

has not been observed experimentally. It involves a volumetric distortion (quantified by a change in lattice parameters)and a local shuffle of the interior Ni and Ti atoms along the $[010]B19$ direction. Table 5.1 shows the lattice paramters and energies calculated for the structures B_2, R-phase $B19$, and $B19'$ which have been used in this work.

Table 5.1: Lattice parameters and energy values for relevant structures in $NiTi$. Calculations were performed using the GGA [55] approximation. Energy difference is computed relative to the B_2 structure in $meV/f.u$

Structure	Space Group	a (Å)	b (Å)	c (Å)	δE (meV/f.u)
B_2	221	3.0075	4.2534	4.2534	0.0
R	148	6.6428	6.6428	6.6428	-29.0
$B19$	51	2.7096	4.2620	4.6450	- 48.2
$B19'$	11	2.9002	4.6349	4.0569	-80.0

While the last few decades have greatly furthered our knowledge of the underlying dynamics of the SME in $Ni - Ti$, the system is still not fully understood. In a ground-breaking paper in 2003, Huang [93] used DFT to show that the ground-state structure of $Ni - Ti$ corresponds to a BCO structure which is vastly different from the monoclinic $B19'$ martensititc low temperature phase. They reasoned that the BCO phase however becomes unstable under shear stress and hydrostatic pressure with respect to monoclinic B19'. This finding was further explained using the concept of the 'Ericksen-Pitteri' neighbourhood (EPN). While undergoing a martensitic transformation, the austenite can give rise to several martensite variants which may combine in twinning and deformation. However, each of these variants or combinations thereof return to a unique parent austenite. The material during the course of the transformation is always within it's EPN and hence is able to store the data

56

necessary for the shape memory effect. The BCO structure however lies on the boundary between two neighbourhoods and is not uniquely reversible and hence cannot store the information necessary for the SME [93]. It was hypothesised that internal stresses arising from the microstructure are responsible for the stabilization of B19' as opposed to the BCO structure. As shown in section 4, to fully understand the phase selection process during such transformations, an exhaustive investigation must be carried out.

A number of attempts have been made to model the transformation from B_2 to the B19' phase in $Ni - Ti$. Kibey et al. [49] presented the energy landscape for the B_2-B19 transformation using a distortion-shuffle 2D model. They also predicted the existence of a finite energy barrier between the B_2 and B19 structures. Their model does not extend to the true martensite B19'. At the same time, Hatcher [94] established a barrierless transformation path for equiatomic $NiTi$ consisting of two consecutive shears: (i) basal shear composed of bilayer $\leq 100 \geq 011$ stacking faults to the B2 phase (i.e. a B_2 - 109° B19') and (ii) another basal shear which causes a relaxation of the structures monoclinic angle and results in the B19' phase (109° B19' - 99° B19'). In 2010, Vishnu et al [95] modeled the $B2 - B19 - B19' - BCO$ transformation by linearly interpolating between the lattice parameters of the parent and martensitic structures using the monoclinic angle (γ) as the reaction coordinate. These simulations predicted a barrierless transformation from B_2-B19-B19'-BCO. Recently, in 2014, Zarkevich et al [96], used the generalized solid state nudged elastic band (GSSNEB) method to model the transformations between the body-centered orthorhombic (BCO) ground state and a newly identified stable austenite (glassy B_2-like) structure [97], intermediate structure (kinematically limited R phase) and between martensite variants B19 and B19'. The GSSNEB path shows a barrierless transformation from $B2 - B19' - BCO$ and the authors also claim that the path

57
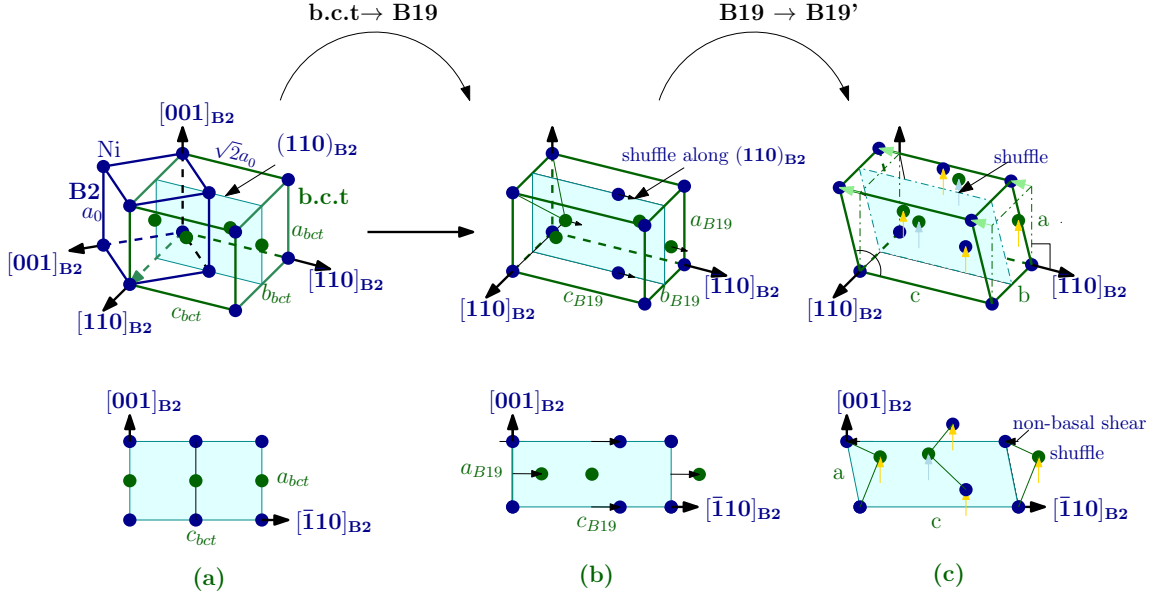
Figure 5.1: Schematic of the B2-B19' transformation

bypasses the $B19$ structure.

5.2   Model Formulation

As is evident from the above discussion, there exists a very grey region in the understanding of the $B2 - B19'$ transformation in $Ni - Ti$. In this work we present a complete parameterized model of the $B2 - B19'$ transformation in $Ni - Ti$. First, we investigate whether the $B19$ phase is an intermediate structure in the transformation or whether the transformation bypasses $B19$ entirely. To do this, we build on the work carried out by Kibey et al. [49], in which they modeled the $B2 - B19$ martensitic transformation using a shuffle-distortion 2-dimensional model. We take their work a step further and also model the $B19 - B19'$ transformation using a monoclinic distortion-shear 2 dimensional model. Figure 5.1 shows a schematic description of the atomic movemenets necessary to generate $B19'$ from $B2$, via the $B19$ phase. The $B2 - B19'$ transformation, using a parent body centred tetragonal

58

(bct) lattice, consists of four independent motions: (i) shuffle along $[110]_{B_2}$, (ii) orthorhombic distortion (change in lattice parameters), (iii) shuffle along $[001]_{B_2}$ and (iv) monoclinic distortion. Assuming that the $B19$ phase is an intermediate phase, this multi-dimensional phase transformation may be attempted in two, 2-dimensional stages (i) $B2 - B19$ and (ii) $B19 - B19'$.

5.2.1 B2 - B19 model
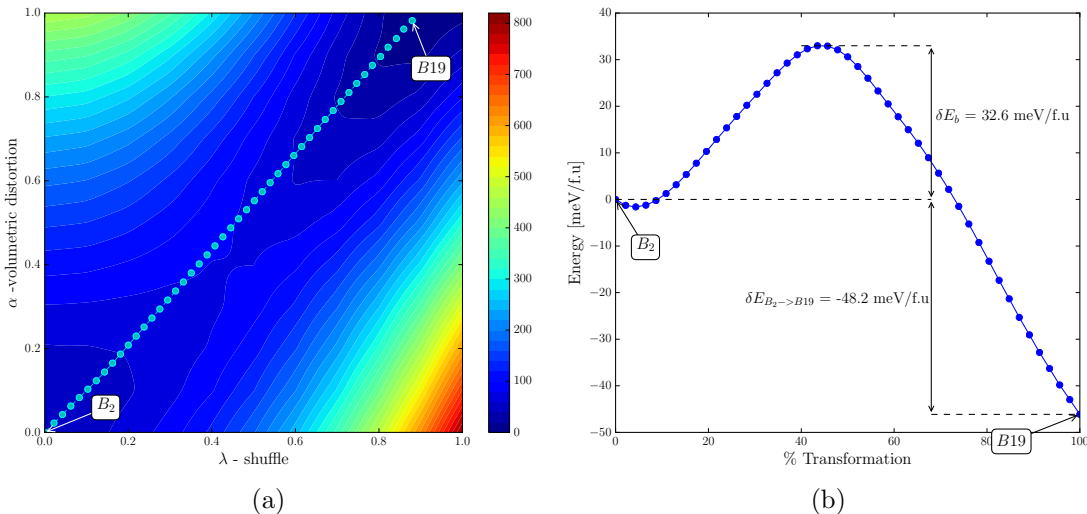
Figure 5.2: (a) Energy landscape, and (b) MEP profile for the $B2 - B19$ transformation in $Ni - Ti$ SMA

The energy landscape for the $B2 - B19$ transformation is shown in Figure 5.2a. Here, $(0,0)$ corresponds to the B_2 structure and $(1,1)$ corresponds to the $B19$ structure. Along the x-axis, we parameterize the shuffle along $[110]_{B_2}$, while the x-axis corresponds to the volumetric distortion. Lattice parameters used are indicated in Table 5.1. Figure 5.2b, shows the energy profile for the minimum energy path (MEP) for the transformation. We see that there exists a small barrier to the transformation

$(\delta_b = 8.4 meV/f.u)$. This agrees with the results reported by Kibey[49], but contradicts the calculations reported by Vishnu et al.[95] who found no energy barrier. It is worth noting, that irrespective of whether the $B19$ phase is an intermediate phase, the linear interpolation technique used in [95] is not a rigorous method to use while modeling such transformations. It would seem to be more exact, to account for all degrees of freedom and model the transformation accordingly, albeit at higher computational cost.

5.2.2   B19 - B19' model
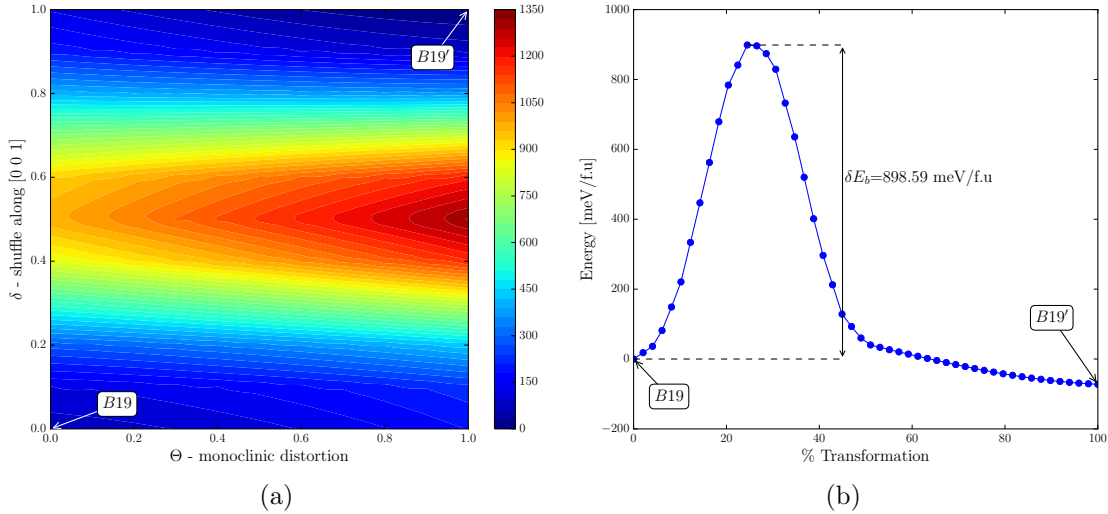
Figure 5.3: (a) Energy landscape, and (b) MEP profile for the $B19 - B19'$ transformation in $Ni - Ti$ SMA

The energy landscape for the $B19 - B19'$ transformation is shown in Figure 5.3. Here, $(0,0)$ corresponds to the $B19$ structure and $(1,1)$ corresponds to the $B19$ structure. Along the x-axis, we parameterize the monoclinic distortion (θ), while the y-axis corresponds to the non-basal shear along the $[110]_{bct}$ direction. θ may

be visualized as monoclinic angle γ varying from 90 - 100°. Lattice parameters used are indicated in Table 5.1. The topology of the enegy lanscape we see here is very interesting. There is a very high energy barrier all along the x-direction, for δ values ranging from 0.3 - 0.7. This essentially means that the $B19 - B19'$ transformation will involve an extremely high, unrealistic barrier. The MEP may be easily visualized as a L - shaped string from $B19$ (0,0) to (0,1) to (1,1). This profile, which would correspond to the lowest energy barrier δ_b (still unrealistically high at $\approx$ 1800 meV/f.u). From this, we may conclude, that it is highly unlikely for the $B19$ phase to be an intermediate structure in the $B2 - B19'$ transformation as reported by [97].

The second approach in the modeling of the transformation, is to directly transform B_2 into $B19'$, incorporating all degrees of freedom. To do this, we start with an initial optimized B_2 structure using a 4 atom base centered tetragonal (bct) lattice. It will undergo four independent, but simultaneous atomic movements: (i) shuffle along $[110]_{B_2}$ (λ), (ii) orthorhombic distortion (change in lattice parameters) (α), (iii) shuffle along $[001]_{B_2}$ (δ)and (iv) monoclinic distortion(θ).

5.2.3   The $B2 - B19'$ transformation model

The end state is the optimized $B19'$ structure. In order to obtain the true $B19'$ structure, initial test runs of the mdoel were carried out to determine the optimal combination of shuffles (along $[110]_{B_2}$ and $[001]_{B_2}$), monoclinic angle and volumetric distortion were carried out bto obtain the lowest energy structure. The $B19'$ structure that was realized, was then relaxed allowing movement of ions. The resultant structure was found to have $\gamma = 97.438$ °. The lattice parameters and energy details are indicated in Table 5.1. To determine the relative volumetric distortion, the model was extended upto 15% volume change. The minimum in the 4-dimensional energy

landscape was isolated at 6.5%. Similarly, the relative shuffles corresponding to the minimum energy were found to be 0.24 in the [001] direction and 0.05 in the [110] direction. A 7x7x7x7 grid was used to populate the energy field, with 1701 point calculations. The domain was then divided into 7 3-parameter energy sets. These point values were then interpolated to generate the 3-dimensional energy field. A steepest descent algorithm implemented via the string method was used to identify the MEP in each of these 7 sets through the energy field. Finite difference method was used to calculate the energy gradient required for the string method. Finally, the 7 separate 3-D MEPs were combined and the resultant data set was used as an initial guess for the 4-dimensional MEP over the entire 4-dimensional energy surface. Selected points were then relaxed allowing movement of ions to generate the final relaxed MEP.

(a) $\delta = 0$ (b) $\delta = 1$
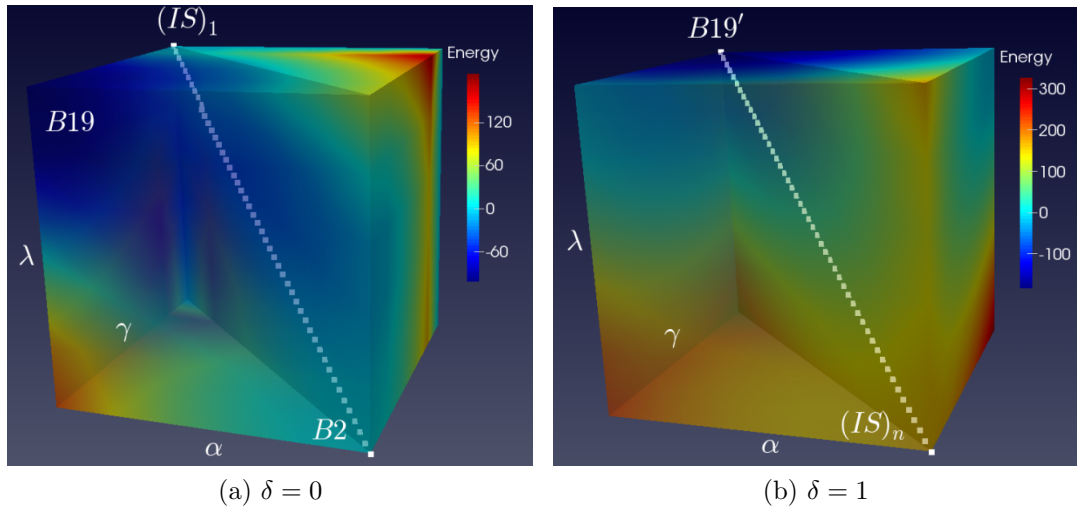
Figure 5.4: 3D energy slice for the B_2-$B19'$ transformation at (a)$\delta = 0$, and (b) $\delta = 1$

For the purpose of visualization, 3-dimensional volume plots are shown in Figures

5.4a and 5.4b. In Figure 5.4a, we see the projection of the MEP in 3-D for $\delta = 0$, i.e a constant value of shuffle along $[001]_{B_2}$, $\delta = 0$. (0,0,0) here corresponds to the B_2 phase. (1,0,1) corresponds to the $B19$ phase, which can be seen to have the lowest energy. However, the MEP is seen to not pass through this point (in agreement with earlier results) since the surrounding landscape proves to be too much of an energy barrier. In Figure 5.4a, we see the projection of the MEP in 3-D for $\delta = 1$, i.e. for a constant value of shuffle along $[001]_{B_2}$, $\delta = 1$.(1,1,1) here corresponds to the $B19'$ phase.
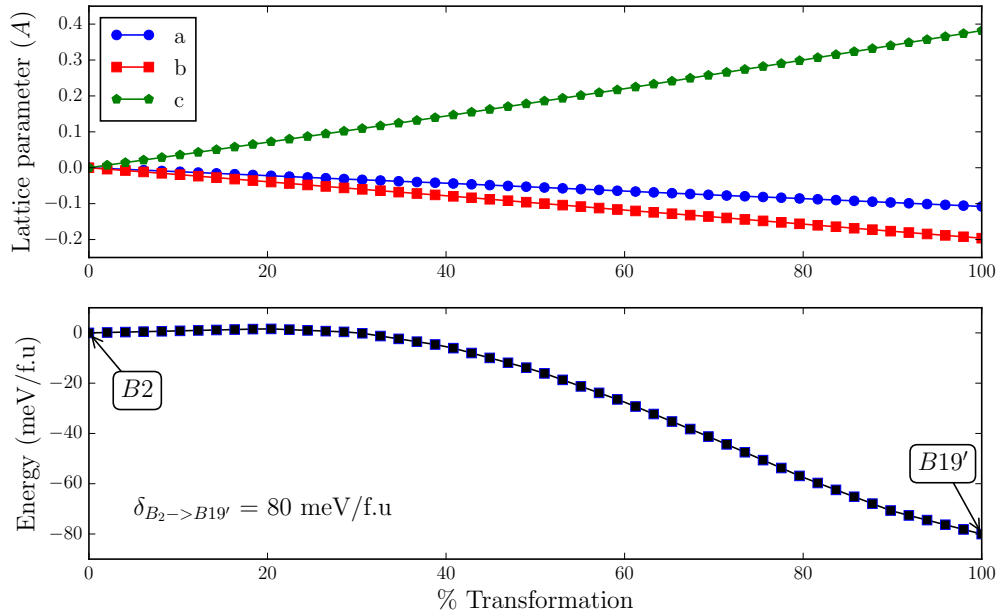
Figure 5.5: Energy profile and lattice parameter variation for the $B2 - B19'$ transformation in $Ni - Ti$

The energy profile along the calculated MEP and the variation in lattice parameters along the transformation is shown in Figure 5.5. The lattice parameters a and c decrease while b increases monotonically during the transformation. This of course,

is an artifact of the tacit assumption in the model that the volumetric distortion is linear. However, this is a reasonable assumption. It is seen from the MEP, that the transformation is barrierless, which agrees with the results reported by [97]. Over the course of the tranformation, it is also seen that the MEP does not pass through the $B19$ structure as well. The results reported here thus completely qualitatively agree with the work of Zarkevich et al [97]. The advantage of this model however lies in the fact that it is not necessary to know the precise lattice parameter of the martensite apriori as opposed to the fact that the GSSNEB is only as good as the initial and final structures provided. Using the 4-dimensional parametric model, given the austenite structure, one may completely model the $B2 - B19'$ transformation and isolate the minimum energy martensite. Also, the model allows complete tracking of independent atom movements and gives a detailed insight into the energetics of the transformation.

5.3   Crystallographic analysis

Figure 5.6 shows the available crystallogrpahic routes for the $B2 - B19'$ transformation calculated using the Bilbao Crystallographic Server [84, 85, 86]. As seen in the figure, there are 12 possible routes which are listed in Table 5.2. The experimentally observed R phase, and the DFT constructs BCO and $B19$ are also indicated in the figure. On analysis of the intermediate structures isolated by the MPE, it is seen that the 4-parameter model yields a martensitic transformation path corresponding to the 10th row in Table 5.2: Pm-3m > P4/mmm > P4/nmm > Pmmn > P21/m. This indicates that the calculated MEP is also crystallographically viable.
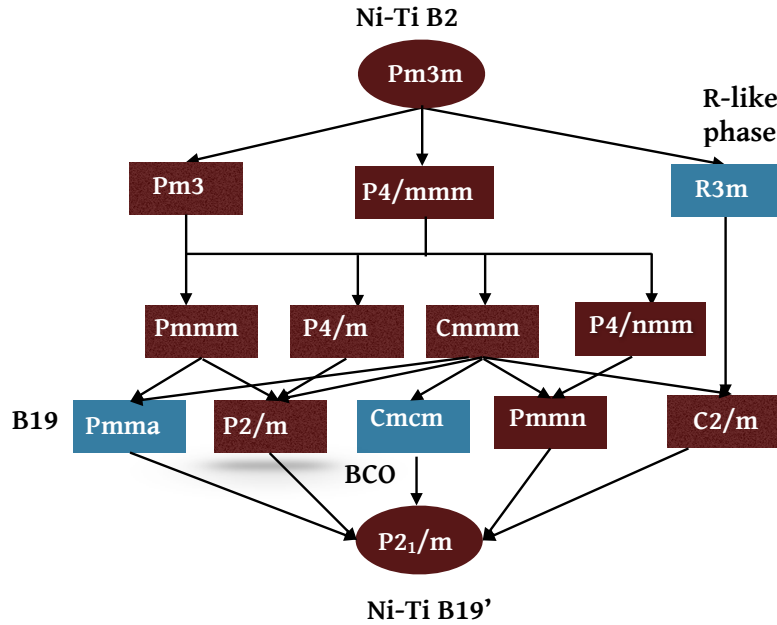
Figure 5.6: Crystallographic routes in $Ni - Ti$ $B2 - B19'$ transformation

Table 5.2: List of crystallographic routes in $Ni - Ti$ $B2 - B19'$ transformation

Sr.No	Route
1	Pm-3m > Pm-3 > Pmmm > Pmma > P2$_1$/m
2	Pm-3m > P4/mmm > Cmmm > Pmmn > P2$_1$/m
3	Pm-3m > P4/mmm > Cmmm > C2/m > P21/m
4	Pm-3m > Pm-3 > Pmmm > P2/m > P21/m
5	Pm-3m > P4/mmm > Pmmm > P2/m > P21/m
6	Pm-3m > P4/mmm > Pmmm > Pmma > P21/m
7	Pm-3m > R-3m > C2/m > P21/m
8	Pm-3m > P4/mmm > Cmmm > P2/m > P21/m
9	Pm-3m > P4/mmm > Cmmm > Cmcm > P21/m
10	Pm-3m > P4/mmm > P4/nmm > Pmmn > P21/m
11	Pm-3m > P4/mmm > P4/m > P2/m > P21/m
12	Pm-3m > P4/mmm > Cmmm > Pmma > P21/m

6. CONCLUDING REMARKS AND FUTURE WORK

The intent of this work is to describe the diffusionless martensitic transformation in transition metal alloys using a combination of shear, shuffle and distortions to parameterize the transformation by accounting for all degrees of freedom. To that end, we investigated three phase transforming systems: (i) Co-based binary alloys, (ii) Co_2NiGa hesuler alloy and (iii) $Ni-Ti$ equiatomic SMA.

6.1 Summary

First, we appled displacive transformation models to Co-based potential shape memory alloys. The f.c.c-b.c.c and f.c.c -h.c.p transformations were modeled for the Co - Al and the Co - Al, Co-Fe, Co-Si systems.. The Bain path calculations for Co - Al showed an energy minimum at a tetragonal structure upto 25 % Al and indicated a theoretical possibility for the f.c.c - b.c.c transformation in Co - Al. The lack of a b.c.c phase in the cobalt phase diagram however, prohibits the expectation of this transformation in this system. Two different parameterized models were used to model the f.c.c - h.c.p structural transformation for three Co-based SMAs. The Wentzcovitch - Lam model predictions agreed with experiments for the Co - Al and the Co-Fe systems. The Shoji-Nishiyama mechanism calculations agreed with experiments for the Co-Fe system. Both mechanisms failed to explain the trends seen in Co-Si. It was concluded that the underlying energetics of the Co-Si system are far removed from those of the Co - Al and Co-Fe systems. We proposed that the martensitic transformation in Co - Al and Co-Fe may be explained by the Wentzcovitch - Lam model. The intermediate structures obtained across both models for all the systems conformed to the common symmetry subgroup theory. This work may be extended to model the energetics and gain a qualitative understanding of the

transformation in Co-based ternary alloys.

Next, we investigated the phase transformation in Co_2NiGa heusler alloy. The Burgers path was investigated. Calculations were carried out using two models: a single-parameter characterization of the Burgers path and a two-parameter Burgers model which generates a transformation energy surface. In both models, a low-energy martensitic structure with an orthorhombic symmetry (O) was observed which has been unobserved experimentally. The Bain path for the alloys was determined and compared to the Burgers path. Minima hopping calculations were carried out to investigate the energy landscapes surrounding the $L1_0$ martensitic phase in $Co - Ni - Ga$. Results showed the existence of a number of structures similar in energy to as well as much lower than the predicted O phase in the vicinity of the $L1_0$ structure. It was postulated the the Co_2NiGa Heusler system exhibits a classic case of the phase selection problem. Although the unexpected Ophase may be relatively more stable than the $L1_0$ phase, the energy barrier for the $L2_1$ -O transformation may be much higher than the barrier to the $L2_1$ -$L1_0$ transformation. In an effort to validate this hypothesis, the stability of this structure was investigated via elastic and lattice dynamics calculations and the contributions of configurational and magnetic disorder on the transformations were studied. No instabilities due to vibrational effects were detected. Elastic calculations showed comparable values of elastic properties for the $L1_0$ and O phases. $C_{11} - C_{12}$ values showed that the O phase is relatively more stable than the $L1_0$ phase. Calculations incorporating configurational disorder showed a lowering in the energy difference between the $L1_0$ and the O structures, but the O structure was still more stable. The calculations simulating the effect of magnetic disorder/ high temperature showed that the $L1_0$ structure may be stabilized with respect to the O phase by lowering the magnetic moment. Thus, it is proposed that magnetic disorder plays an important role in the phase selection energetics

of the $CoNiGa$ system and is a principal contributor in the determination of the transformation path followed in this system. Further calculations were carried out on an off-stoichiometric composition $Co_{43.75}Ni_{25}Ga_{31.25}$, where the weakening of the magnetic ordering manifests naturally. As expected, the $L1_0$ phase was seen to be more stable than the O phase. These results indicate that it is unrealistic to use standard DFT prototypes to investigate ground states of relatively less known systems. By performing a detailed analysis of the transformation paths (Burgers and Bain) by taking into account perturbations on the ground state, it is seen that what is manifested is in principle a phase selection problem: the ultimate crystal structure that the system transforms into, depends on the path that the system prefers. When coming from high temperature, the accessible path is that corresponding to the Bain transformation. To conclude, discrepancies between DFT and experiments may be reconciled if we consider the "history" of the alloy.

$Ni-Ti$ is one of the most widely studied SMAs, yet there is no definite conclusive knowledge about the $B2-B19'$ martensitic transformation which results in the shape memory effect. With an objective of filling this gap, in Section 5, we presented parameterized models for three transformations:, (i) $B2-B19$, (ii) $B19-B19'$ and finally (iii) $B2-B19'$ in Ni-Ti. The $B2-B19$ model was a re-calculation of earlier work by Kibey et al. Kibey et al.[49] which showed that an energy barrier exists in the $B2-B19$ transformation (32.6 meV). The $B19-B19'$ transformation showed a very high energy barrier which indicates that it is highly unlikely that the $B19$ phase is an intermediate phase in the transformation. This conclusion agrees with recent work by Zarkevich [96]. Finally, we presented a complete 4-parameter distortion-shuffle model for the B_2-B19' transformation in Ni-Ti SMA which is the first of it's kind. Earlier models have either modeled only part of the transformation, or applied uni-dimensional linear interpolation models. No earlier model has been able

to depict the entire energy landscape for the transformation. The advantage of this model over prior work is that it is not necessary to know the lattice parameters and angles of the final martensite apriori. The calculated MEP over the parameterized energy landscape was seen to be barrierless, confirming the known instability of the $B2$ structure. $B19'$ was identified as a local minimum in the landscape, again, in consensus with experimental work. It was shown that the $B19$ phase, while crystallographically possible, is not a likely intermediate phase in the transformation. Finally, the obtained MEP is shown to follow a viable crystallogrpahic route.

6.2   Future Work

The framework laid down in this dissertation may be used in the design of high temperature shape memory alloys. The various models implemented may be applied to any new potential HTSMA to determine it's tendency to undergo a martensitic phase transformation. The energetics of the transformation along with the calculated energy barriers may be used to predict the associated hysteresis. The effect of alloying on the energy barrriers of the transformation may be determined, which in turn may be used to predict the effect on M_s of the material. The family of Heusler alloys is vast and as yet unexplored. The phase stability analysis methodology detailed in Section 4 serves as a prototype for the investigation of Heusler alloy systems. The search for new Heusler HTSMA's can be streamlined by following the process outlined. Future work will include the investigation of hitherto unexplored Heusler alloys using this work to discover and develop new HTSMAs.These calculations will be done using high-throughput methods and will contribute to the building of a Heusler materials database. The $B2 - B19'$ model will be extended to model the transformation in ternary $Ni - Ti - Hf$, $Ni - Ti - Zr$, $Ni - Ti - Pt$, and $Ni - Ti - Pd$, using SQS structures, which are potential new HTSMA's. The effect of increased alloying of

Hf,Zr,Pt, and Pd on the energy barrriers of the transformation will be determined and used to predict the hysteresis and the effect on M_s of the material.

REFERENCES

[1] M. Cohen, G.B. Olson, and P.C. Clapp. On the classification of displacive phase transformations. In *Proceedings of International Conference on Martensitic Transformations, ICOMAT-79*, page 1, 1979.

[2] P.A. Lindgård. Theory and modeling of the martensitic transformation. *Le Journal de Physique IV*, 1(C4):C4–3, 1991.

[3] Z. Nishiyama, M.E. Fine, M. Meshii, and C.M. Wayman. *Martensitic transformation*. Academic Press, New York, 1978.

[4] L.C. Chang and T.A. Read. Elastic deformation and diffusionless phase changes in metals-the gold-cadmium betaface. *American Institute of Mining and Metallurgical Engineers*, 191:47, 1951.

[5] Z.S. Basinski and J.W. Christian. Experiments on the martensitic transformation in single crystals of indium-thallium alloys. *Acta Metallurgica*, 2(1):148–166, 1954.

[6] W. J. Buehler, J. V. Gilfrich, and R. C. Wiley. Effect of low - temperature phase changes on the mechanical properties of alloys near composition tini. *Journal of Applied Physics*, 34(5):1475–1477, 1963.

[7] T. Tadaki, K. Otsuka, and K. Shimizu. Shape memory alloys. *Annual Review of Materials Science*, 18(1):25–45, 1988.

[8] John Wyrill Christian. *The theory of transformations in metals and alloys*. Newnes, Oxford, 2002.

[9] Ranjani V. Krishnan, Luc Delaey, H. Tas, and H. Warlimont. Thermoplasticity, pseudoelasticity and the memory effects associated with martensitic trans-

formations Part I: Structural and microstructural changes associated with the transformations. *Journal of Materials Science*, 9(9):1536–1544, 1974.

[10] Ranjani V. Krishnan, Luc Delaey, H. Tas, and H. Warlimont. Thermoplasticity, pseudoelasticity and the memory effects associated with martensitic transformations Part II: The macroscopic mechanical behaviour. *Journal of Materials Science*, 9(9):1536–1544, 1974.

[11] Ranjani V. Krishnan, Luc Delaey, H. Tas, and H. Warlimont. Thermoplasticity, pseudoelasticity and the memory effects associated with martensitic transformations Part III: Thermodynamics and Kinetics. *Journal of Materials Science*, 9(9):1545–1555, 1974.

[12] Erwin Schrödinger. An undulatory theory of the mechanics of atoms and molecules. *Physical Review*, 28(6):1049, 1926.

[13] Walter Kohn. Nobel lecture: Electronic structure of matter-wave functions and density functionals. *Reviews of Modern Physics*, 71(5):1253–1266, 1999.

[14] Lewellyn H. Thomas. The calculation of atomic fields. In *Mathematical Proceedings of the Cambridge Philosophical Society*, volume 23, pages 542–548. Cambridge Univ Press, 1927.

[15] Enrico Fermi. Un metodo statistico per la determinazione di alcune priorieta dell'atome. *Rend. Accad. Naz. Lincei*, 6(602-607):32, 1927.

[16] Pierre Hohenberg and Walter Kohn. Inhomogeneous electron gas. *Physical review*, 136(3B):B864, 1964.

[17] Walter Kohn and Lu Jeu Sham. Self-consistent equations including exchange and correlation effects. *Physical Review*, 140(4A):A1133, 1965.

[18] John P. Perdew and Alex Zunger. Self-interaction correction to density-functional approximations for many-electron systems. *Physical Review B*, 23(10):5048, 1981.

[19] John P. Perdew, Kieron Burke, and Yue Wang. Generalized gradient approximation for the exchange-correlation hole of a many-electron system. *Physical Review B*, 54(23):16533, 1996.

[20] Georg Kresse and Jürgen Hafner. *Ab initio* molecular dynamics for liquid metals. *Physical Review B*, 47(1):558, 1993.

[21] Georg Kresse and Jürgen Hafner. *Ab initio* molecular-dynamics simulation of the liquid-metal–amorphous-semiconductor transition in germanium. *Physical Review B*, 49(20):14251, 1994.

[22] Georg Kresse and Furthmüller Jürgen. Efficiency of *ab initio* total energy calculations for metals and semiconductors using a plane-wave basis set. *Computational Materials Science*, 6(1):15–50, 1996.

[23] Georg Kresse and Jürgen Furthmüller. Efficient iterative schemes for *ab initio* total-energy calculations using a plane-wave basis set. *Physical Review B*, 54(16):11169, 1996.

[24] R.P. Feynman. Forces in molecules. *Physical Review*, 56(4):340, 1939.

[25] H. Hellmann. Einfuhrung in die quantumchemie. *Franz Deutsche, Leipzig*, page 285, 1937.

[26] P. E. Blöchl. Projector augmented-wave method. *Phys. Rev. B*, 50:17953–17979, Dec 1994.

[27] Siqing Wei and M.Y. Chou. *Ab initio* calculation of force constants and full phonon dispersions. *Physical review letters*, 69(19):2799, 1992.

[28] Gerardo Damián Garbulsky. *Ground-state structure and vibrational free energy in first-principles models of subsitutional-alloy thermodynamics.* PhD thesis, Massachusetts Institute of Technology, 1996.

[29] Xavier Gonze. First-principles responses of solids to atomic displacements and homogeneous electric fields: Implementation of a conjugate-gradient algorithm. *Physical Review B*, 55(16):10337, 1997.

[30] Xavier Gonze and Changyol Lee. Dynamical matrices, born effective charges, dielectric permittivity tensors, and interatomic force constants from density-functional perturbation theory. *Physical Review B*, 55(16):10355, 1997.

[31] A. Van de Walle, M. Asta, and G. Ceder. The alloy theoretic automated toolkit: A user guide. *Calphad*, 26(4):539–553, 2002.

[32] S. Ganeshan, S.L. Shang, Y. Wang, and Z.K. Liu. Effect of alloying elements on the elastic properties of Mg from first-principles calculations. *Acta Materialia*, 57(13):3876–3884, 2009.

[33] S. Ganeshan, S.L. Shang, H. Zhang, Y. Wang, M. Mantina, and Z.K. Liu. Elastic constants of binary Mg compounds from first-principles calculations. *Intermetallics*, 17(5):313–318, 2009.

[34] S.L. Shang, A. Saengdeejing, Z.G. Mei, D.E. Kim, H. Zhang, S. Ganeshan, Y. Wang, and Z.K. Liu. First-principles calculations of pure elements: Equations of state and elastic stiffness constants. *Computational Materials Science*, 48(4):813–826, 2010.

[35] Yvon Le Page and Paul Saxe. Symmetry-general least-squares extraction of elastic data for strained materials from *ab initio* calculations of stress. *Physical Review B*, 65(10):104104, 2002.

[36] Thien Duong, Sean Gibbons, Rajeev Kinra, and Raymundo Arróyave. *Ab initio* approach to the electronic, structural, elastic, and finite-temperature thermodynamic properties of Ti_2AX (A= Al or Ga and X= C or N). *Journal of Applied Physics*, 110(9):093504–093504, 2011.

[37] E. Weinan, Weiqing Ren, and Eric Vanden-Eijnden. String method for the study of rare events. *Physical Review B*, 66(5):052301, 2002.

[38] Hannes Jónsson, Greg Mills, and Karsten W Jacobsen. Nudged elastic band method for finding minimum energy paths of transitions. *Classical and quantum dynamics in condensed phase simulations*, 1:385–404, 1998.

[39] E. Weinan, Weiqing Ren, and Eric Vanden-Eijnden. Simplified and improved string method for computing the minimum energy paths in barrier-crossing events. *The Journal of Chemical Physics*, 126(16):164103, 2007.

[40] Stefan Goedecker. Minima hopping: an efficient search method for the global minimum of the potential energy surface of complex molecular systems. *The Journal of chemical physics*, 120:9911–9917, 2004.

[41] Frank Jensen. *Introduction to computational chemistry.* John Wiley & Sons, West Sussex, 2007.

[42] Yuri N. Koval. High temperature shape memory effect in some alloys and compounds. In *Materials science forum*, volume 327, pages 271–278. Trans Tech Publ, 2000.

[43] P. Tolédano, G. Krexner, M. Prem, H.P. Weber, and V.P. Dmitriev. Theory of the martensitic transformation in cobalt. *Physical Review B*, 64(14):144104, 2001.

[44] T. Omori, Y. Sutou, K. Oikawa, R. Kainuma, and K. Ishida. Shape memory effect associated with fcc-hcp martensitic transformation in co-al alloys. *Materials transactions-JIM*, 44(12):2732–2735, 2003.

[45] JW Christian. A theory of the transformation in pure cobalt. *Proceedings of the Royal Society of London. Series A. Mathematical and Physical Sciences*, 206(1084):51–64, 1951.

[46] Z.S. Basinski and J.W. Christian. The martensitic transformation in cobalt. *Philosophical Magazine*, 44(354):791–792, 1953.

[47] W. Bollmann. On the phase transformation of cobalt. *Acta Metallurgica*, 9(10):972–975, 1961.

[48] R.M. Wentzcovitch and P.K. Lam. Fcc-to-hcp transformation: A first-principles investigation. *Physical Review B*, 44(17):9155, 1991.

[49] S. Kibey, H. Sehitoglu, and D.D. Johnson. Energy landscape for martensitic phase transformation in shape memory NiTi. *Acta Materialia*, 57(5):1624–1629, 2009.

[50] T. Qian, W. Ren, and P. Sheng. Current dissipation in thin superconducting wires: A numerical evaluation using the string method. *Physical Review B*, 72(1):014512, 2005.

[51] A. Samanta. Modified string method for finding minimum energy path. *Arxiv preprint arXiv:1009.5612*, 2010.

[52] I. Folkins and M.B. Walker. Configuration-space approach to the fcc to hcp structural transition. *Physical Review Letters*, 65(1):127–130, 1990.

[53] E.C. Bain. The nature of martensite. *Trans AIME Steel Div*, 70:25–46, 1924.

[54] W.G. Burgers. On the process of transition of the cubic-body-centered modification into the hexagonal-close-packed modification of zirconium.

[55] John P. Perdew and Yue Wang. Accurate and simple analytic representation of the electron-gas correlation energy. *Phys. Rev. B*, 45:13244–13249, Jun 1992.

[56] H.J. Monkhorst and J.D. Pack. Special points for brillouin-zone integrations. *Physical Review B*, 13(12):5188–5192, 1976.

[57] M. Methfessel and A.T. Paxton. High-precision sampling for brillouin-zone integration in metals. *Physical Review B*, 40(6):3616, 1989.

[58] P.E. Blöchl, O. Jepsen, and O.K. Andersen. Improved tetrahedron method for brillouin-zone integrations. *Physical Review B*, 49(23):16223, 1994.

[59] J. Ma, I. Karaman, and R.D. Noebe. High temperature shape memory alloys. *International Materials Reviews*, 55(5):257–315, 2010.

[60] M. Siewert, M. E. Gruner, A. Dannenberg, A. Hucht, S. M. Shapiro, G. Xu, D. L. Schlagel, T. A. Lograsso, and P. Entel. Electronic structure and lattice dynamics of the magnetic shape-memory alloy Co_2NiGa. *Physical Review B*, 82(6):064420, 2010.

[61] X.F. Dai, G. D. Liu, Z. H. Liu, G. H. Wu, J. L. Chen, F. B. Meng, H. Y. Liu, L. Q. Yan, J. P. Qu, and Y. X. Li. Superelasticity of CoNiGa: Fe single crystals. *Applied Physics Letters*, 87(11):112504–112504, 2005.

[62] Jian Liu, Mingxu Xia, Yanlu Huang, Hongxing Zheng, and Jianguo Li. Effect of annealing on the microstructure and martensitic transformation of magnetic shape memory alloys CoNiGa. *Journal of alloys and compounds*, 417(1):96–99, 2006.

[63] E. Dogan, I. Karaman, Y. I. Chumlyakov, and Z. P. Luo. Microstructure and martensitic transformation characteristics of CoNiGa high temperature shape memory alloys. *Acta Materialia*, 59(3):1168–1183, 2011.

[64] Demircan Canadinc, Jayaram Dadda, Hans Jürgen Maier, Ibrahim Karaman, Haluk E. Karaca, and Yuriy I. Chumlyakov. On the role of the cooling rate and crystallographic orientation on the shape memory properties of CoNiAl single crystals under compression. *Smart materials and structures*, 16(4):1006, 2007.

[65] K. Oikawa, L. Wulff, T. Iijima, F. Gejima, T. Ohmori, A. Fujita, K Fukamichi, R. Kainuma, and K. Ishida. Promising ferromagnetic Ni–Co–Al shape memory alloy system. *Applied Physics Letters*, 79(20):3290–3292, 2001.

[66] Y. Murakami, D. Shindo, K. Oikawa, R. Kainuma, and K. Ishida. Magnetic domain structures in Co–Ni–Al shape memory alloys studied by Lorentz microscopy and electron holography. *Acta materialia*, 50(8):2173–2184, 2002.

[67] Antje Dannenberg. *Ab initio and Monte Carlo investigations of structural, electronic and magnetic properties of new ferromagnetic Heusler alloys with high Curie temperatures*. PhD thesis, Universität Duisburg-Essen, Fakultät für Physik Theoretische Physik, 2011.

[68] Takahiro Yamada, Takuji Ikeda, Ralf P. Stoffel, Volker L Deringer, Richard Dronskowski, and Hisanori Yamane. Synthesis, crystal structure, and high-temperature phase transition of the novel plumbide Na2MgPb. *Inorganic chemistry*, 53(10):5253–5259, 2014.

[69] Jian Liu, Hua Xie, Yanqiu Huo, Hongxing Zheng, and Jianguo Li. Microstructure evolution in CoNiGa shape memory alloys. *Journal of alloys and compounds*, 420(1):145–157, 2006.

[70] Tina Fichtner, Changhai Wang, Aleksandr Levin, Guido Kreiner, Catalina-Salazar Mejia, Simone Fabbrici, Franca Albertini, and Claudia Felser. Effects of annealing on the martensitic transformation of Ni-based ferromagnetic shape memory heusler alloys and nanoparticles. *Metals*, 5(2):484–503, 2015.

[71] Pierre Tolédano and Vladimir Dmitriev. *Reconstructive phase transitions*. World Scientific, Singapore, 1996.

[72] W. G. Burgers. On the process of transition of the cubic-body-centered modification into the hexagonal-close-packed modification of zirconium. *Physica*, 1(7-12):561–586, 1934.

[73] Anubhav Jain, Shyue Ping Ong, Geoffroy Hautier, Wei Chen, William Davidson Richards, Stephen Dacek, Shreyas Cholia, Dan Gunter, David Skinner, Gerbrand Ceder, and Kristin A. Persson. The Materials Project: A materials genome approach to accelerating materials innovation. *APL Materials*, 1(1):011002, 2013.

[74] James E. Saal, Scott Kirklin, Muratahan Aykol, Bryce Meredig, and C. Wolverton. Materials Design and Discovery with High-Throughput Density Functional Theory: The Open Quantum Materials Database (OQMD). *JOM*, 65(11):1501–1509, 2013.

[75] S Curtarolo, G.L.W. Hart, W. Setyawan, M. Mehl, M. Jahnatek, R.V. Chepulskii, O. Levy, and D. Morgan. Aflow: software for high-throughput calculation of material properties, 2009.

[76] John P. Perdew and Alex Zunger. Self-interaction correction to density-functional approximations for many-electron systems. *Physical Review B*, 23(10):5048, 1981.

[77] M. Friák and M. Šob. *Ab initio* study of the bcc-hcp transformation in iron. *Physical Review B*, 77(17):174117, 2008.

[78] M. Šob, M. Friák, L.G. Wang, and V. Vitek. *Ab initio* study of changes in the magnetism of iron during the bcc-hcp phase transformation. In *MRS Proceedings*, volume 538, Cambridge, 1998. Cambridge Univ Press.

[79] M. Šob, M. Friák, L. Wang, and V. Vitek. Elastic compatibility, martensitic textures and weak plasticity. In *Proceedings of the International Conference on Solid-Solid Phase Transformations 99 (JIMIC-3)*, pages 855–858. The Japan Institute of Metals, 1999.

[80] S.R. Nishitani, H. Kawabe, and M. Aoki. First-principles calculations on bcc–hcp transition of titanium. *Materials Science and Engineering: A*, 312(1):77–83, 2001.

[81] Maximilian Amsler and Stefan Goedecker. Crystal structure prediction using the minima hopping method. *J. Chem. Phys.*, 133:224104–1 – 224104–8, 2010.

[82] Michele Parrinello and Aneesur Rahman. Polymorphic transitions in single crystals: A new molecular dynamics method. *Journal of Applied physics*, 52(12):7182–7190, 1981.

[83] John P. Perdew, Kieron Burke, and Matthias Ernzerhof. Generalized gradient approximation made simple. *Phys. Rev. Lett.*, 77:3865–3868, Oct 1996.

[84] Mois I. Aroyo, J.M. Perez-Mato, D. Orobengoa, E. Tasci, G. De La Flor, and A. Kirov. Crystallography online: Bilbao crystallographic server. *Bulg. Chem. Commun*, 43(2):183–97, 2011.

[85] Mois I. Aroyo, Juan Manuel Perez-Mato, Cesar Capillas, Eli Kroumova, Svetoslav Ivantchev, Gotzon Madariaga, Asen Kirov, and Hans Wondratschek. Bil-

bao Crystallographic Server: I. Databases and crystallographic computing programs. *Zeitschrift für Kristallographie*, 221(1/2006):15–27, 2006.

[86] Mois I. Aroyo, Asen Kirov, Cesar Capillas, J.M. Perez-Mato, and Hans Wondratschek. Bilbao Crystallographic Server. II. Representations of crystallographic point groups and space groups. *Acta Crystallographica Section A: Foundations of Crystallography*, 62(2):115–128, 2006.

[87] Kaushik Bhattacharya. Theory of martensitic microstructure and the shape-memory effect. In *Shape-memory alloys: from microstructure to macroscopic properties*. Trans Tech Publications, 1998.

[88] Navdeep Singh, Ebubekir Dogan, Ibrahim Karaman, and Raymundo Arróyave. Effect of configurational order on the magnetic characteristics of Co–Ni–Ga ferromagnetic shape memory alloys. *Physical Review B*, 84(18):184201, 2011.

[89] Eduard Obradó, Lluis Mañosa, and Antoni Planes. Stability of the bcc phase of Cu–Al–Mn shape-memory alloys. *Phys. Rev. B*, 56:20–23, Jul 1997.

[90] V. Recarte, J. I. Pérez-Landazábal, V. Sánchez-Alarcos, and J. A. Rodríguez-Velamazán. Dependence of the martensitic transformation and magnetic transition on the atomic order in Ni–Mn–In metamagnetic shape memory alloys. *Acta Materialia*, 60(5):1937–1945, 2012.

[91] Alex Zunger, S.H. Wei, L. G. Ferreira, and James E. Bernard. Special quasirandom structures. *Physical Review Letters*, 65(3):353, 1990.

[92] Kazuhiro Otsuka and Xiabing Ren. Physical metallurgy of Ti-Ni-based shape memory alloys. *Progress in materials science*, 50(5):511–678, 2005.

[93] X. Huang, G.J. Ackland, and K.M. Rabe. Crystal structures and shape-memory behaviour of NiTi. *Nature Materials*, 2(5):307–311, 2003.

[94] N. Hatcher, O. Yu Kontsevoi, and A.J. Freeman. Martensitic transformation path of NiTi. *Physical Review B*, 79(2):020202, 2009.

[95] Karthik Guda Vishnu and Alejandro Strachan. Phase stability and transformations in niti from density functional theory calculations. *Acta Materialia*, 58(3):745–752, 2010.

[96] Nikolai A Zarkevich and Duane D Johnson. Shape-memory transformations of niti: Minimum-energy pathways between austenite, martensites, and kinetically limited intermediate states. *Physical review letters*, 113(26):265701, 2014.

[97] Nikolai A Zarkevich and Duane D Johnson. Stable atomic structure of NiTi austenite. *Physical Review B*, 90(6):060102, 2014.